Copyrighted Materials
Copyright © 2010 SciTech Publishing Retrieved from www.knovel.com

CHAPTER 16

Constant False Alarm Rate Detectors

Byron Murray Keel

Chapter Outline

16.1 INTRODUCTION

The process of detecting a target begins with comparing a radar measurement with a threshold. Measurements exceeding the threshold are associated with returns from a target, and measurements below the threshold are associated with thermal noise or other interference sources including intentional jamming and background returns from terrain and bodies of water. The detector threshold is selected to achieve the highest possible probability of detection for a given signal-to-noise ratio (SNR) and probability of false alarm. A false alarm occurs when, in the absence of a target, a source of interference produces a measured value that exceeds the detection threshold. A radar system is designed to achieve and maintain a specified probability of false alarm. False alarms drain radar resources by appearing as valid target detections requiring subsequent radar actions and thus degrade system performance.

If the statistics of the interference are known a priori, a threshold may be selected to achieve a specific probability of false alarm. In many cases, the form of the probability density function (PDF) associated with the interference is known, but the parameters of the distribution are either unknown or change temporally or spatially. Constant false alarm rate (CFAR) detectors are designed to track changes in the interference and to adjust the detection threshold to maintain a constant probability of false alarm.

16.2 OVERVIEW OF DETECTION THEORY

An introduction to constant false alarm rate detectors begins with a review of detection theory. Detection decisions are based on measurements of reflected signals received at the radar and thermal noise inherently present in the receiver. Samples or measurements may be collected in one or more dimensions, including range, cross-range, angle, and Doppler. In general, the received signals are sampled at an interval spacing equal to the radar system's resolution in the dimension in which they are collected. The radar detector is tasked with comparing the measurement with a threshold and choosing between two hypotheses. Measurements exceeding the threshold are declared to contain returns from targets as well as energy from interfering sources and are associated with the target-plus-interference hypothesis (commonly referred to as the H_1 hypothesis). Measurements below the threshold are declared to contain energy only from interfering sources and are associated with the null hypothesis, H_0. Interfering sources include receiver noise, intentional jamming, unintentional electromagnetic interference, and background returns (often referred to as "clutter"). Clutter returns are defined as reflections from objects in the scene that are not viewed as "targets" by the radar (e.g., reflections from precipitation or terrain).

A diagram of a radar's basic processing chain is provided in Figure 16-1. The analog-to-digital converter (ADC) converts the received analog signal into digital samples. Signal conditioning is then applied to these samples to maximize the signal-to-interference-plus-noise-ratio (SINR) prior to the detector. Signal conditioning algorithms include, but are not limited to, Doppler processing, pulse compression, array processing, and space-time adaptive processing (see Chapters 17 and 20). In general, these algorithms operate on complex samples. The real and imaginary parts of a complex sample correspond to the receiver's in-phase (I) and quadrature (Q) channels. Complex signals at the output of the conditioning process are then passed to a rectifier. A rectifier converts the complex samples into either their magnitude or magnitude-squared values. A linear rectifier outputs a complex sample's magnitude, and a square law rectifier outputs its magnitude squared. A detector employing a linear (or square law) rectifier is referred to as a linear (or square law) detector. A log rectifier may also be applied [1,2]. A log rectifier compresses the dynamic range of the measured values and is less susceptible to target masking. Target masking refers to missed detections caused by target returns that bias the CFAR detection threshold. Target masking and its impact on CFAR detection performance are examined in detail in subsequent sections.

The detector operates on the output of the rectifier and yields one of three possible outcomes: a correct decision, a missed detection, or a false alarm. A correct decision is one in which the detector correctly declares the presence or absence of a target. A missed detection is one in which the detector declares the absence of a target when in truth the measurement contains a target return. A false alarm occurs when the detector declares the presence of a target and in reality a target's return is not present in the measured data.

In radar, both interference and target returns are modeled as random processes characterized by PDFs and power spectral densities or, equivalently, autocorrelation functions.

FIGURE 16-1 ■ In a modern radar, the processing chain operates on digital data to maximize SINR, detect targets, and control false alarms.

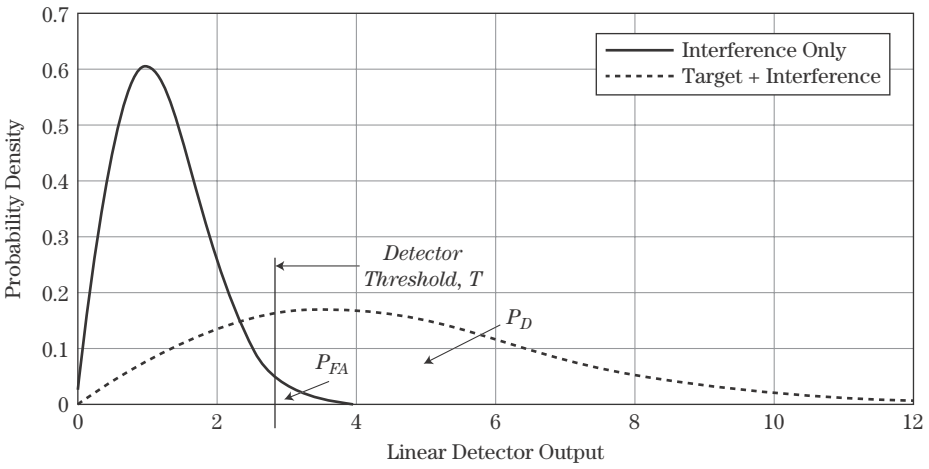

FIGURE 16-2 ■ Setting the detector threshold determines the P_{FA} of the null hypothesis and the P_D of the target present hypothesis.

In many cases, both the target and interference are Rayleigh distributed at the output of a linear rectifier [3]. Figure 16-2 contains a plot of the PDF associated with Rayleigh distributed interference (solid curve) and a plot of the PDF associated with a Swerling 1 or 2 [3] target combined with Rayleigh distributed interference (dashed curve). Section 15.5.9 showed that, in the absence of noncoherent integration (i.e., $N = 1$), both a Swerling 1 and 2 target produce a Rayleigh distributed voltage at the output of a linear rectifier.

Due to the stochastic nature of target returns and interference, a detector's performance is described in terms of probabilities. The likelihood of detecting a target is specified in terms of a probability of detection, P_D, and the likelihood of a false alarm is specified in terms of a probability of false alarm, P_{FA}. A detector may be designed to optimize performance based on a cost function that weights each decision (i.e., correct decision, missed detection, and false alarm).

The Neyman-Pearson (NP) detector, described in Chapter 15, employs a fixed threshold that maximizes P_D given a specific probability of false alarm. The NP detector is employed assuming that the interference is independent and identically distributed (IID) over all resolution cells to which the fixed threshold is to be applied and that the parameters of the interference distribution are known. In many cases, the assertion that the distribution parameters are known is not valid. The solution is to employ a detector that estimates the parameters of the distribution from the measured data and uses the estimate to set the detector threshold. This chapter focuses on methods for adaptively setting the detector threshold to maintain a constant false alarm rate.

Once a threshold, T, has been selected, performance metrics such as P_D and P_{FA} may be computed using the target-plus-interference and interference-only PDFs. P_D is calculated by computing the area under the target-plus-interference PDF to the right of the threshold, and P_{FA} is calculated by computing the area under the interference-only PDF to the right of the threshold. The area under each PDF associated with P_D and P_{FA} is illustrated in Figure 16-2. In general, threshold selection is a trade-off between P_D and P_{FA} for a given SINR and the cost associated with a correct and incorrect decision.

The occurrence of a false alarm represents a drain on limited radar resources. The frequency of false alarms has a direct impact on overall radar system performance and is quantified using a false alarm rate metric. *False alarm rate* is defined as the number of

false alarms occurring within a given time interval. False alarm rate, *FAR*, is computed using the expression

$$FAR = \frac{P_{FA} M}{T_M} = N_D P_{FA} \tag{16.1}$$

where M represents the number of resolution cells collected over a specific time interval defined by T_M and $N_D = M/T_M$ is the number of detection decisions per unit time.

16.3 FALSE ALARM IMPACT AND SENSITIVITY

The initial task assigned to a radar system is to detect targets. Once a target is detected, radar resources are then allocated to other functions such as verification, track initiation, discrimination, or the measurement of some physical property associated with the target. False alarms cause the radar to invoke actions that consume finite resources. For example, verify pulses or track initiate pulses may be commanded in response to false alarms and as a result reduce the time available for other actions. A large number of false alarms may also overload the data bus and signal/data processor, which would result in dropped detections or tracks and a reduction in the timeline and processing capacity available for other radar modes (e.g., discrimination). Radars are often sized to accommodate a specific false alarm rate. A significant increase in the false alarm rate produces a substantial decrease in system performance.

In most cases, changes in the false alarm rate correspond to fluctuations in the interference power. For example, thermal noise power in the receiver may vary with time due to internal heating and cooling as well as to changes in ambient radiation impinging on the antenna. Interference power levels may also fluctuate due to intentional jamming or variations in terrain reflectivity associated with changes in terrain type or grazing angle.

A square law detector is commonly applied in radar systems and exhibits several desirable properties. In many instances, the PDFs at the output of a square law detector and the resulting mathematical analysis are relatively tractable. In addition, for Rayleigh distributed interference, the maximum likelihood (ML) estimator of the mean interference power takes the form of a square law detector. The mean power estimate is used as a statistic in a number of the CFAR algorithms examined in subsequent sections.

Interference that is Rayleigh distributed at the output of a linear detector will be exponentially distributed at the output of a square law detector, as shown in equation (15.10) and repeated here [3],

$$p_z(z) = \begin{cases} \dfrac{1}{\sigma_i^2} \exp\left(\dfrac{-z}{\sigma_i^2}\right), & z \geq 0 \\ 0, & z < 0 \end{cases} \tag{16.2}$$

where $z = |y|^2$ is the output of the detector when its input is the complex interference signal y, and σ_i^2 is the mean or expected value of z. The output of a square law detector is interpreted as a power measurement, whereas the output of a linear detector is interpreted as a voltage measurement. Thus, the quantity σ_i^2 represents the mean of the interference power. Given exponentially distributed interference, the probability of a false alarm is

computed by integrating equation (16.2) from the threshold T to $+\infty$, or

$$P_{FA} = \int_{T}^{\infty} \frac{1}{\sigma_i^2} \exp\left(-\frac{z}{\sigma_i^2}\right) dz \tag{16.3}$$

which gives

$$P_{FA} = \exp\left(-\frac{T}{\sigma_i^2}\right) \tag{16.4}$$

For a fixed threshold, an increase in the interference power causes an increase in P_{FA} as evident in equation (16.4).

Suppose that the mean interference power is increased by a factor of κ and that the threshold is not adjusted. The threshold is initially set based on a desired probability of false alarm and an assumed interference power. Using equation (16.4), the probability of false alarm resulting from an increase in the interference power is

$$P_{FA_{final}} = (P_{FA_{initial}})^{1/\kappa} \tag{16.5}$$

where $P_{FA_{initial}}$ is the initial probability of false alarm, and $P_{FA_{final}}$ is the resultant probability of false alarm. Consider an increase in the interference power by a factor of 3 dB (i.e., $\kappa = 2$). In this case, $P_{FA_{final}} = \sqrt{P_{FA_{initial}}}$. For $P_{FA_{initial}} = 10^{-4}$, or 1 false alarm per 10,000 observations, the probability of false alarm increases to 10^{-2}, or 1 false alarm in 100 observations. This example illustrates a dramatic increase in probability of false alarm or false alarm rate for a relatively small increase in interference power. As expected, P_{FA} increases because the threshold is not adjusted to account for the increase in the interference power.

16.4 CFAR DETECTORS

A desirable property of a detector is an ability to maintain a given probability of false alarm in the presence of heterogeneous or changing interference. A detector possessing this property is termed a constant false alarm rate detector. CFAR detectors estimate statistics of the interference from radar measurements and adjust the detector threshold to maintain a constant false alarm rate or, equivalently, a fixed P_{FA}.

In response to increasing interference, it can be argued that a higher threshold maintains the false alarm rate at a cost of degraded detection performance. This argument is valid, but there are other ways to increase the probability of detection once the threshold is adjusted. If the interference is associated with thermal noise or a noise jammer, one option is to increase the pulse length in order to place more energy on target and thus increase the SNR. As discussed in Chapters 3 and 15, P_D increases with increasing SNR.

An examination of CFAR algorithms begins with the cell-averaging (CA) CFAR [4]. The CA-CFAR exhibits optimum performance in a homogeneous interference environment. In many operational environments, heterogeneous conditions exist including spatial and temporal variations in the interference power and closely spaced target returns that may bias the threshold estimate. CFAR algorithms designed to operate in heterogeneous environments include greatest-of [5-7], smallest-of [6-8], censored [9,10], and order statistic [11,12] CFARs. These and other CFAR algorithms are examined in subsequent sections.

16.4.1 Review of the Neyman-Pearson Square Law Detector

Before describing the CA-CFAR algorithm in more detail, it is useful to examine the Neyman-Pearson detector and its properties [13]. An NP detector maximizes P_D given a desired P_{FA}. The threshold is fixed and is derived from a known interference PDF. In applying the NP detector, it is assumed that the interference environment is homogenous and that the parameters of the distribution are known.

Chapter 15 developed the NP detector for different combinations of linear and square law detectors; nonfluctuating and fluctuating targets; and coherent or noncoherent integration. In all cases, complex Gaussian interference was assumed. In this chapter, the focus is restricted to square law detectors and single-pulse or coherent integration processing. Noncoherent integration is not applied. Under these conditions, the likelihood ratio [13] reveals that the optimum form of the detector for a Swerling 1 or 2 target is square law. Swerling 1 and 2 targets exhibit exponentially distributed radar cross section fluctuations.

Now consider a Swerling 1 target embedded in Rayleigh distributed interference. Under the null hypothesis H_0, the in-phase and quadrature channels contain normally distributed interference and are modeled as

$$y = \mathrm{I}_i + j\mathrm{Q}_i \tag{16.6}$$

where $\mathrm{I}_i \sim \mathrm{N}\left(0, \sigma_i^2/2\right)$ and $\mathrm{Q}_i \sim \mathrm{N}\left(0, \sigma_i^2/2\right)$, respectively. Under the H_1 hypothesis, the receiver output is modeled as

$$y = (\mathrm{I}_i + \mathrm{I}_t) + j\,(\mathrm{Q}_i + \mathrm{Q}_t) \tag{16.7}$$

where $\mathrm{I}_t \sim \mathrm{N}\left(0, \sigma_t^2/2\right)$, and $\mathrm{Q}_t \sim \mathrm{N}\left(0, \sigma_t^2/2\right)$. The subscripts i and t denote interference and target, respectively. The output, z, of a square law detector under hypothesis H_0 (interference only) is exponentially distributed according to the PDF given in equation (16.2). The output for the target-plus-interference case is also exponentially distributed [3]

$$p_z(z) = \begin{cases} \dfrac{1}{\sigma_i^2 + \sigma_t^2} \exp\left(\dfrac{-z}{\sigma_i^2 + \sigma_t^2}\right), & z \geq 0 \\ 0, & z < 0 \end{cases} \tag{16.8}$$

It is common to write equation (16.8) in terms of SINR

$$p_z(z) = \begin{cases} \dfrac{1}{\sigma_i^2\,(1 + SINR)} \exp\left(\dfrac{-z}{\sigma_i^2\,(1 + SINR)}\right), & z \geq 0 \\ 0, & z < 0 \end{cases} \tag{16.9}$$

where $SINR = \sigma_t^2/\sigma_i^2$.

A Neyman-Pearson detector maximizes P_D under the constraint of achieving a specific probability of false alarm. The threshold is derived by solving equation (16.4) for the threshold T, yielding

$$T = -\ln(P_{FA})\sigma_i^2 \tag{16.10}$$

The threshold consists of the product of two terms. The first term is a function of the desired P_{FA}, and the second, σ_i^2, represents the interference power at the output of the square law detector.

Similarly, a CFAR detector's threshold is expressed, in general, as the product of two terms

$$T = \alpha \hat{g} \tag{16.11}$$

where $\hat{g}$ is a statistic associated with the interference and is estimated from the measured data, and α is the CFAR constant and is a function of the desired P_{FA}. These parameters will be examined in more detail in subsequent sections.

Computing the threshold in equation (16.10) for a specific P_{FA} requires knowledge of the interference power. As previously discussed, in many scenarios the interference power is not known a priori and may vary both temporally and spatially. In addition, small increases in interference power can produce significant increases in the false alarm rate. A detector designed to adapt its threshold to changing interference levels is required if a constant false alarm rate is to be achieved in practice.

16.4.2 Basic CFAR Architecture

In this section, the basic architecture and elements associated with a CFAR algorithm are examined. A generic CFAR detector is depicted in Figure 16-3. The samples at the output of the rectifier are stored in a data window for presentation to the detector. The CFAR window resides within the data window and is composed of leading and lagging reference windows, guard cells (Gs), and a cell under test (CUT).

Data and CFAR windows may be single- or multidimensional. An example of a one-dimensional (1-D) window is a range window consisting of N_R resolutions cells. A generic, 1-D data sequence and CFAR window are illustrated in Figure 16-4. An example

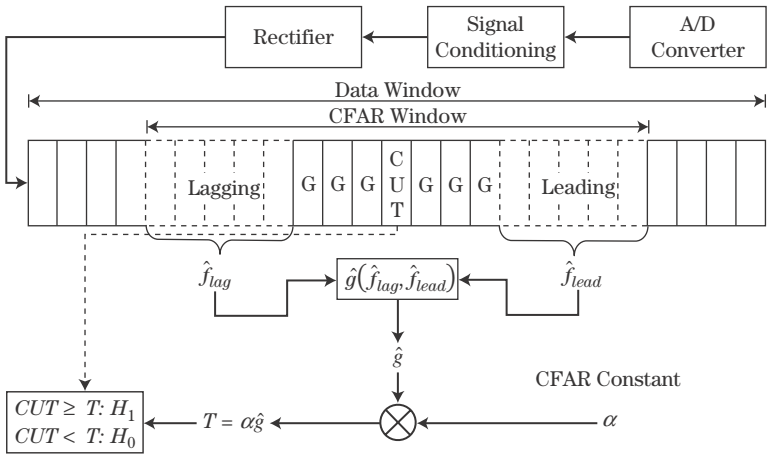

FIGURE 16-3 ■ The Constant-False-Alarm Rate (CFAR) detector uses measured samples to derive a threshold designed to maintain a constant P_{FA} in heterogeneous environments.

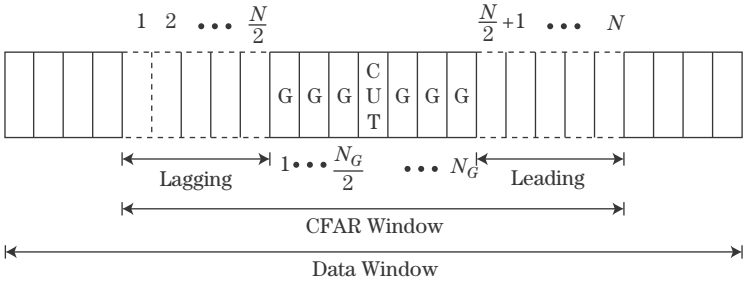

FIGURE 16-4 ■ The one-dimensional CFAR window is a subset of the data window.

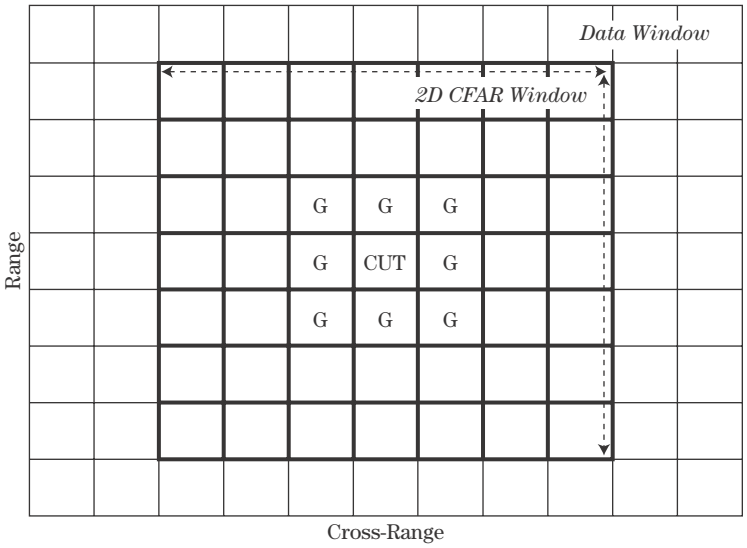

FIGURE 16-5 ■ An area CFAR uses two-dimensional data and CFAR windows.

of a two-dimensional (2-D) data set is a synthetic aperture radar (SAR) image consisting of N_R range and N_{CR} cross-range cells. A 2-D data set and CFAR window are depicted in Figure 16-5.

In Figure 16-4, the CUT is located in the center of the CFAR window. The term *cell under test* refers to the current cell to which the CFAR threshold is to be applied. In general, a fixed number of resolution cells on either side of the cell under test are denoted as *guard* or *gap cells* (indicated by a "G" in Figure 16-4). Measurements contained in the guard cells are not used to estimate the interference statistic, as they may contain returns associated with the target in the cell under test, which will bias the interference estimate. Reference windows are defined outside the guard cell region and are denoted in the 1-D case as the *leading* and *lagging windows*. The leading window is defined as the window in the direction of movement through the data window. Measurements contained in the reference windows are used to estimate the interference statistic.

The CFAR window is moved through the data window one sample or cell at a time. At each position, a detection decision is made regarding the measurement in the CUT. The detection threshold applied to the CUT is derived from measurements contained in the leading and lagging windows.

The question of how to apply the detector to the cells located within $N/2$ samples of the ends of the data window is often asked. For those cells, the CUT is not required to lie midway between the leading and lagging windows and may be shifted within the CFAR window, resulting in a nonsymmetric window. The CFAR algorithms examined in this chapter assume a symmetric CFAR window but can be modified to account for asymmetry. Note that some algorithms process the two reference windows separately and compute individual interference statistics. In these cases, extra care is needed when deriving thresholds and performance bounds for asymmetric windows. In general, it is desirable to maintain equal length reference windows (leading and lagging) but to allow the CUT and guard cells to be repositioned within the reference window if needed to test for targets at the beginning and end of the data window.

A CFAR window may be defined and applied in two dimensions (e.g., range and cross-range), as shown in Figure 16-5. For the 2-D case, the labels "leading" and "lagging" may

be less intuitive, but this does not prevent the cells from being partitioned into two windows. A 2-D CFAR is commonly applied to a SAR image to detect targets or regions of interest. Detection is possible since the returns from targets are, in general, larger than returns from neighboring terrain. Over a large area, the returns from terrain may appear heterogeneous, but over localized regions, the terrain is often homogeneous, thus accommodating some form of CFAR processing.

In some systems, where measurements are collected over multiple dimensions (e.g., fast time and slow time), the CFAR detector may be applied in only a single dimension. For example, consider a moving target detector employing both range and Doppler processing. In many cases, the Doppler dimension is partitioned into *endo-* and *exo-clutter* regions. The endo-clutter region is heterogeneous in nature, and a clutter boundary exists between the two regions. In these cases, the Doppler dimension is less conducive to CFAR processing, and the CFAR is applied in only the range dimension.

Referring to the CFAR architecture in Figure 16-3, the interference statistics are computed independently for the leading and lagging windows and are denoted $\hat{f}_{lead}$ and $\hat{f}_{lag}$, respectively. The two statistics are combined using one of a number of possible operations, including mean, minimum, or maximum, to form a composite statistic, $\hat{g}$. A CFAR constant, α, is selected based on a desired P_{FA} and is a function of both the P_{FA} and specific CFAR parameters (e.g., reference window size). The threshold, T, is defined by the product of the CFAR constant, α, and the composite interference statistic, $\hat{g}$. Once the threshold has been estimated, it is applied to the CUT, and a detection decision is made. Next, the CFAR window is shifted by one resolution cell, and the process is repeated until a detection decision is made for each cell within the data window.

16.5 CELL AVERAGING CFAR

The cell averaging CFAR was first introduced by Finn and Johnson [4] in 1968. The algorithm is relatively simple in that it computes a threshold based on an estimate of the average interference power in the reference window. The CA-CFAR is designed to operate in a fairly benign interference/target environment. The following assertions are made when applying a CA-CFAR:

1. The interference in the leading and lagging windows and in the CUT is IID.
2. With a target return present in the CUT, the leading and lagging windows do not contain returns from other targets that bias the threshold estimate.

Environments for which these conditions hold are labeled "homogeneous." For many real-world target/clutter environments, these conditions are too restrictive, and a more robust CFAR algorithm is required. CFAR algorithms designed to operate in heterogeneous environments are examined in subsequent sections.

The CA-CFAR is derived to illustrate the steps involved in developing a CFAR algorithm and to identify the limitations and performance bounds associated with the detector. The derivation is based on several assertions:

1. The interference in the reference window and CUT is IID.
2. The interference is Rayleigh distributed in voltage.
3. The rectifier is square law, and thus the interference at the output is exponentially distributed.

4. The mean of the interference power at the output of the rectifier is unknown and must be estimated from the samples in the reference window.
5. The target is modeled as either a Swerling 1 or 2 (Rayleigh voltage).

The first step in the derivation is to compute an estimate of the average interference power using the samples in the reference window. The interference at the output of the square law detector is exponentially distributed

$$p_z(z) = \frac{1}{\sigma_i^2} \exp\left(\frac{-z}{\sigma_i^2}\right) \quad z \geq 0 \tag{16.12}$$

where σ_i^2 is the mean of the interference power. For the samples in the reference window, the joint PDF is

$$p_z(z) = \frac{1}{\left(\sigma_i^2\right)^N} \exp\left(-\sum_{n=1}^{N} z_n \Big/ \sigma_i^2\right) \quad z_n \geq 0 \tag{16.13}$$

where $z = \{z_1, z_2, \ldots, z_N\}$. Given the joint PDF, the maximum likelihood estimate [14] of the interference power is

$$\hat{\sigma}_i^2 = \frac{1}{N} \sum_{n=1}^{N} z_n \tag{16.14}$$

The CA-CFAR applies the maximum likelihood estimator in (16.14) to the samples in the leading and lagging windows to form an estimate of the interference power.

The CA-CFAR threshold, T_{CA}, is defined by the product of the power estimate in equation (16.14) and the CA-CFAR constant, α_{CA}, or

$$T_{CA} = \alpha_{CA} \hat{\sigma}_i^2 \tag{16.15}$$

The CFAR constant is a function of both the desired P_{FA} and the number of samples in the reference window. An expression relating the three parameters, α_{CA}, P_{FA}, and N, is defined in subsequent paragraphs.

The next step is to compute the average probability of detection as a function of the estimated threshold. The probability of detection is obtained by integrating the PDF in equation (16.9) from the estimated threshold to infinity. Given the CA-CFAR threshold in (16.15), the PDF in (16.9) may be integrated to obtain the probability of detection for a Swerling 1 or 2 target

$$P_D = \int_{\alpha_{CA}\hat{\sigma}_i^2}^{\infty} \frac{1}{\sigma_i^2(1 + SINR)} \exp\left(\frac{-z}{\sigma_i^2(1 + SINR)}\right) dz \tag{16.16}$$

or

$$P_D\left(\hat{\sigma}_i^2\right) = \exp\left(\frac{-\alpha_{CA}\hat{\sigma}_i^2}{\sigma_i^2\,(1 + SINR)}\right) \tag{16.17}$$

The probability of detection defined in (16.17) is a function of the interference power estimate, which is a random variable, and thus $P_D\left(\hat{\sigma}_i^2\right)$ is also a random variable. To compute the average probability of detection, the PDF associated with the interference

power estimate is required and is defined by [3,15]

$$p_{\hat{\sigma}_i^2}\left(\hat{\sigma}_i^2\right) = \frac{N^N \left(\hat{\sigma}_i^2\right)^{N-1} \exp\left(\dfrac{-N\hat{\sigma}_i^2}{\sigma_i^2}\right)}{\left(\sigma_i^2\right)^N (N-1)!} \quad \hat{\sigma}_i^2 \geq 0 \tag{16.18}$$

The average or mean probability of detection, $\bar{P}_D$, is found by integrating (16.17) over all possible values of the interference statistic defined in (16.18), or

$$\bar{P}_D = \int_0^\infty p_{\hat{\sigma}_i^2}(\hat{\sigma}_i^2) \exp\left(\frac{-\alpha_{CA}\hat{\sigma}_i^2}{\sigma_i^2(1+SINR)}\right) d\hat{\sigma}_i^2 \tag{16.19}$$

Using the fact that [16]

$$\int_0^\infty x^n \exp(-ax)dx = \frac{n!}{a^{n+1}} \tag{16.20}$$

where x is a real valued variable, $a > 0$, and n is a positive integer, it can be shown [3] that (16.19) reduces to a simple closed-form expression

$$\bar{P}_D = \left[1 + \frac{\dfrac{\alpha_{CA}}{N}}{(1+SINR)}\right]^{-N} \tag{16.21}$$

The average probability of false alarm is found by setting *SINR* equal to zero, corresponding to the interference-only condition. This gives

$$\bar{P}_{FA} = \left[1 + \frac{\alpha_{CA}}{N}\right]^{-N} \tag{16.22}$$

Note that the average probability of false alarm is independent of the interference power. The detector thus achieves a constant false alarm rate without a priori knowledge of the interference power. This property is used to define a "CFAR" detector.

As a notational convenience, the overbar on P_D and P_{FA} will not be used in the remainder of this chapter. The reader should remember that when referring to the performance of a CFAR detector, references to P_D and P_{FA} denote an average probability obtained by integrating over all possible values of the interference statistic.

The CA-CFAR constant is found by solving for α_{CA} in (16.22), giving

$$\alpha_{CA} = N\left[P_{FA}^{-1/N} - 1\right] \tag{16.23}$$

This expression for the CFAR constant applies only to the cell-averaging case and should not be associated with other CFAR algorithms.

In some cases, the number of operations is reduced by defining an interference statistic that is not normalized by $1/N$

$$\hat{g}'_{CA} = \sum_{n=1}^{N} z_n \tag{16.24}$$

and incorporating the $1/N$ factor into the CFAR constant. For this case, the resultant CFAR constant is defined by

$$\alpha'_{CA} = \left[P_{FA}^{-1/N} - 1\right] \tag{16.25}$$

and the CA-CFAR threshold is expressed as

$$T_{CA} = \alpha'_{CA}\hat{g}'_{CA} \tag{16.26}$$

16.5.1 CA-CFAR Performance

In the following sections, the performance of a CA-CFAR is examined in terms of CFAR loss, target masking, and clutter boundaries. In a homogeneous environment, the CA-CFAR is designed to achieve an average probability of false alarm. The uncertainty or variance in the CFAR statistic produces a threshold that is greater than the threshold associated with the NP detector for the same P_{FA}. The higher threshold implies that an SINR greater than that associated with an NP detector is required to achieve a given P_D. In a radar system, the CFAR detector's higher SINR requirement is interpreted as a "loss," since the lower SINR associated with the NP detector is not sufficient to achieve the desired P_D when applying the CFAR threshold. "CFAR loss" is defined as the ratio of the SINR required by a CFAR detector to that required by an NP detector for a given P_D and should be accounted for in the radar system design.

In a heterogeneous environment, multiple targets and changes in the interference power degrade CFAR performance. Target returns in the reference window bias the threshold estimate and may prevent the target in the cell under test from being detected. This condition is known as *target masking*. *Clutter boundaries* are defined by significant, localized changes in the interference power. The occurrence of a clutter boundary may lead to an increased number of false alarms and to masking of targets located near the boundary.

16.5.2 Homogeneous Performance

A numerical example is used to examine the performance of a CA-CFAR operating in a homogenous environment. Consider a single target embedded in IID interference. The measured returns and CA-CFAR threshold are plotted in Figure 16-6. The data window consists of 1,000 cells, and a Swerling 1 target is positioned in the 500th cell. The target is embedded in Rayleigh distributed interference with an average $SINR = 20$ dB. The

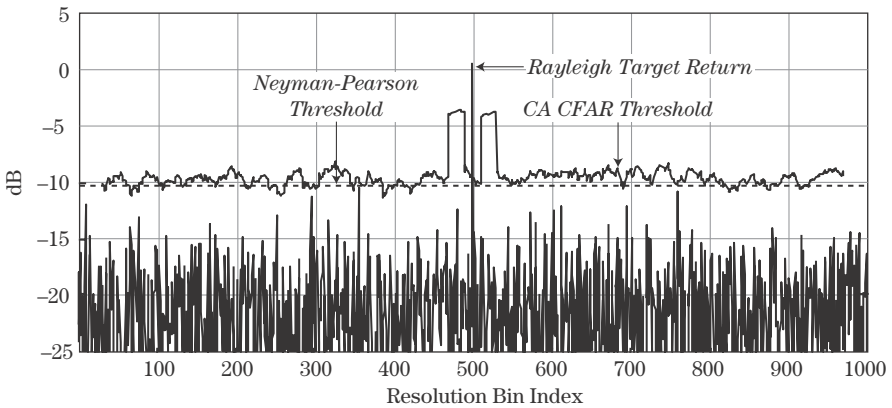

FIGURE 16-6 ■ The Cell-Averaging (CA)-CFAR ($N = 40$, $N_G = 20$, $P_{FA} = 10^{-4}$) varies the threshold over the data window containing a single target with $SINR = 20$ dB.

CFAR parameters are $N = 40$, $N_G = 20$, and $P_{FA} = 10^{-4}$. A large value of N_G is chosen to illustrate the influence of guard cells on the CFAR threshold.

The plot compares the CFAR-derived threshold (solid curve) with the Neyman-Pearson threshold (dashed curve), which requires knowledge of the interference power. The target's return exceeds both the CFAR and NP threshold. A number of the interference samples are close to the CFAR threshold, but in this realization none exceed the threshold. This is not surprising since the probability of a false alarm is 1 in 10,000, but only 1,000 cells were examined. The CA-CFAR exhibits a threshold that, in general, exceeds the threshold of the NP detector. The higher CA threshold translates into a larger SINR requirement, compared with the NP detector, to achieve a given P_D.

The impact of a target return located in either the leading or lagging reference window is illustrated in Figure 16-6. As the CFAR window moves to the right, the target initially falls in the leading window and subsequently appears in the lagging window. The presence of a target return in either reference window biases the threshold higher. Note that when the target return falls in either the CUT or the guard cell region, the return is not used in computing the interference statistic. A target present in the reference window imposes a bias on the threshold that may mask a target in the CUT. This condition is referred to as *mutual target masking.*

16.5.3 CFAR Loss

As observed in Figure 16-6, the CA-CFAR threshold appears, on average, to be higher than the NP threshold. The higher threshold leads to a reduction in P_D. To achieve a P_D equivalent to that of the NP detector requires a higher SINR. The ratio of the *SINR* required for a CA-CFAR detector to that required for an NP detector, for a given value of P_D and P_{FA}, is defined as the CFAR loss.

Expressions for P_D and P_{FA} are derived for the NP detector using equations (16.3) and (16.9), respectively. P_{FA} is defined by

$$P_{FA} = \exp\left(\frac{-T}{\sigma_i^2}\right) \tag{16.27}$$

and P_D is defined by

$$P_D = \exp\left(\frac{-T}{\sigma_i^2\,(1 + SINR)}\right) \tag{16.28}$$

Solving for *SINR* as a function of P_D and P_{FA} yields

$$SINR_{NP} = \frac{\ln\left(\frac{P_{FA}}{P_D}\right)}{\ln(P_D)} \tag{16.29}$$

where $SINR_{NP}$ is the SINR associated with the NP detector. Equation (16.29) defines the SINR required to achieve a specified value of P_D and P_{FA} when employing an NP detector.

For a CA-CFAR detector, the SINR required to achieve a specified value of P_D and P_{FA} is derived from equations (16.21) and (16.22) and is

$$SINR_{CA} = \frac{\left(\frac{P_D}{P_{FA}}\right)^{1/N} - 1}{1 - (P_D)^{1/N}} \tag{16.30}$$

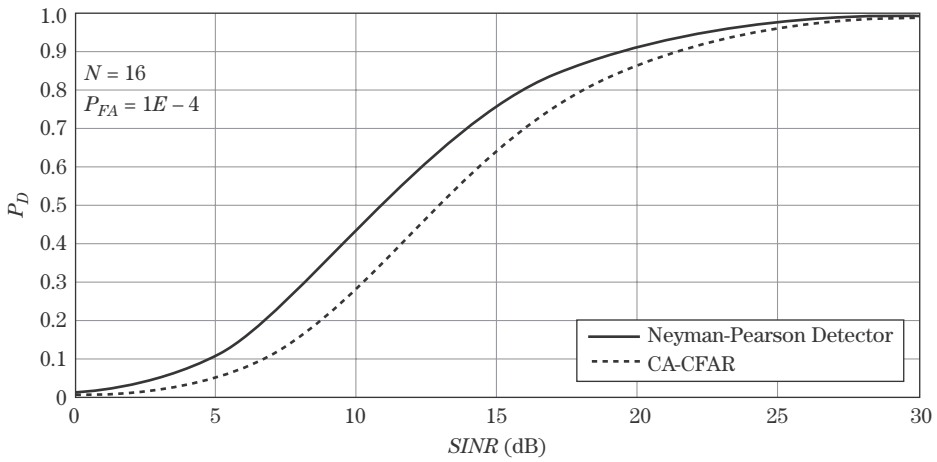

FIGURE 16-7 ■ ROC for a Neyman-Pearson detector and CA-CFAR. Additional *SINR* is required for a given P_D when employing CA-CFAR.

Note that the required *SINR* is a function of three parameters: P_D, P_{FA}, and N. Equation (16.30) is valid only for a Swerling 1 or 2 target and does not apply to noncoherently integrated returns. For a CA-CFAR, CFAR loss is defined as

$$L_{CA\text{-}CFAR} = \frac{SINR_{CA}}{SINR_{NP}} \tag{16.31}$$

In general, CFAR loss is defined as

$$L_{CFAR} = \frac{SINR_{CFAR}}{SINR_{NP}} \tag{16.32}$$

where $SINR_{CFAR}$ is the SINR associated with a given CFAR algorithm.

Receiver operating characteristic (ROC) curves are used in radar to relate SINR and detection performance. Receiver operating curves for the NP and CA-CFAR detectors are derived using (16.29) and (16.30), respectively, and are provided in Figure 16-7. The curves are based on $P_{FA} = 10^{-4}$ and $N = 16$. The location of the CA-CFAR ROC, which is to the right of the NP ROC, is indicative of a higher SINR requirement for a given P_D. CFAR loss is, therefore, the difference in SINR between the two ROCs for a given P_D. For 90% P_D, the CA-CFAR loss is ~2 dB in this example.

CFAR loss is a function of three parameters: P_D, P_{FA}, and N. For a given P_D, CFAR loss decreases with increasing P_{FA} and increasing N. The dependence on N is illustrated in Figure 16-8 for three values of P_{FA} (10^{-4}, 10^{-6}, and 10^{-8}) and 90% P_D. The decrease in CFAR loss corresponding to an increase in N is intuitive in that the variance in the interference power estimate decreases with increasing N, thus leading to a more accurate estimate of the interference power. As the CFAR loss decreases or equivalently as N increases, CFAR performance approaches that of the NP detector [6].

Based on the previous discussion, a large reference window could be used to minimize CFAR loss. A problem with this assertion is that as the size of the reference window is increased, the likelihood of encompassing multiple targets or a heterogeneous interference environment also increases. For example, a large reference window increases the likelihood that two or more targets will reside within the CFAR window and thus increases the potential for mutual target masking. Typically, the number of bins comprising the reference window ranges from 20 to 40, but this number varies depending on the resolution of the system and the target/interference environment.

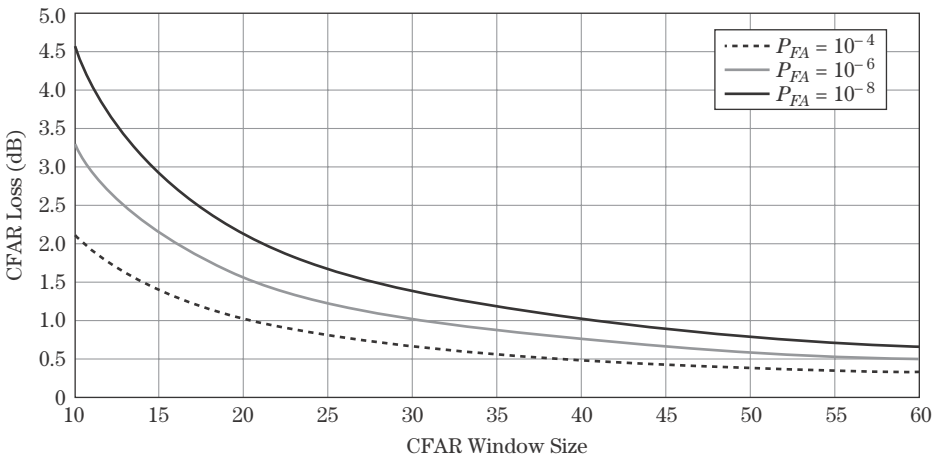

FIGURE 16-8 ■ CFAR loss as a function of CA-CFAR window size for three different values of P_{FA} and a 90% P_D.

Robust CFARs, examined in subsequent sections, are designed to operate in heterogeneous environments. The robustness of these algorithms is achieved at a price that includes greater CFAR loss and a higher degree of complexity and increased computational expense.

16.5.4 CA-CFAR Performance in Heterogeneous Environments

In this section, the performance of a CA-CFAR is examined under various heterogeneous conditions. Heterogeneous conditions exist when either of the following is true:

1. Target returns are present in either, or both, the leading or lagging windows and a target is simultaneously present in the CUT.
2. Interference sources are not identically distributed throughout the entire reference window.

Target returns in the reference window may arise from two sources:

1. A target located in the CUT whose physical extent occupies several resolution bins (e.g., a 3 m length target occupying three 1 m resolution bins).
2. Multiple targets.

In general, these heterogeneous conditions degrade CFAR performance resulting in either a loss in P_D or increase in P_{FA}. In the next two sections, the impact of targets and clutter boundaries on CA-CFAR performance is examined.

16.5.4.1 Masking

Target masking occurs when target returns located within the reference window bias the threshold above the return in the CUT. Target masking may be partitioned into two categories: self-masking and mutual target masking.

Self-masking is associated with an extended target. An extended target is defined as one whose physical extent causes it to occupy more than one resolution cell. With a sample of an extended target located in the CUT, the remaining samples associated with the target bias the threshold if one or more samples lie within the reference window. The biased threshold may mask the presence of the extended target resulting in *self-masking*.

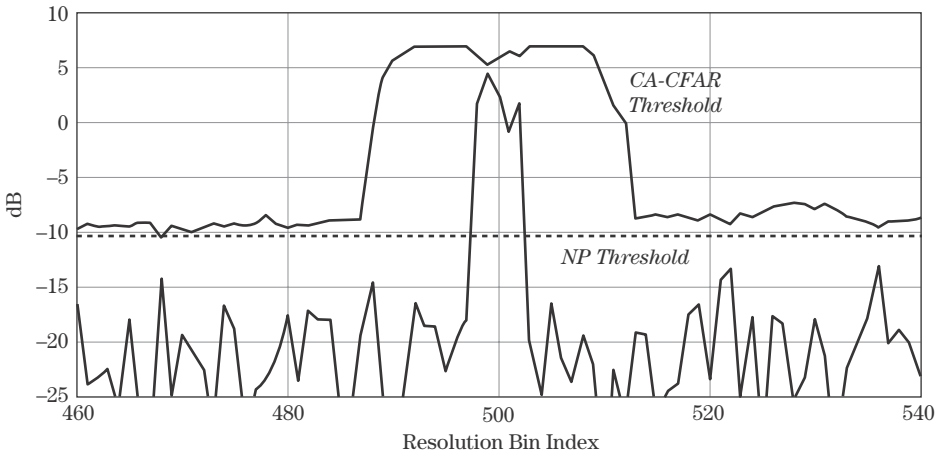

FIGURE 16-9 ■ A CA-CFAR ($N = 20$) with no guard cells exhibits self-masking when an extended target consisting of 5 Rayleigh distributed scatterers is encountered.

An example of self-masking is illustrated in Figure 16-9. The extended target is composed of five Rayleigh distributed scatterers, each occupying a different resolution cell. A CA-CFAR is applied with $N = 20$ and no guard cells for illustration. The CFAR threshold is biased above the target, and none of the target's samples are detected. The extended target experiences self-masking.

Guard or gap cells may be added to both sides of the CUT to suppress self-masking. Figure 16-10 contains a plot of the previous data set with a new threshold obtained using a CFAR window consisting of 16 guard cells ($N_G = 16$), eight on each side of the CUT, and $N = 20$. As is evident from the plot, the guard cells prevent self-masking. The number of guard cells employed is a function of the maximum target extent and the resolution of the system. The minimum number of guard cells to place on either side of the CUT is equal to the target's extent divided by the resolution cell size.

Mutual target masking occurs when target returns not associated with the target in the CUT fall within the reference window and bias the threshold. To illustrate mutual target masking, the returns from two Swerling 1 targets are plotted in Figure 16-11. The Swerling targets have an average SINR equal to 20 dB. The targets are point targets and are separated by 10 resolution cells. A CA-CFAR is applied with $N = 20$ and $N_G = 16$. In Figure 16-11, the target on the right masks the presence of the target on the left. The target

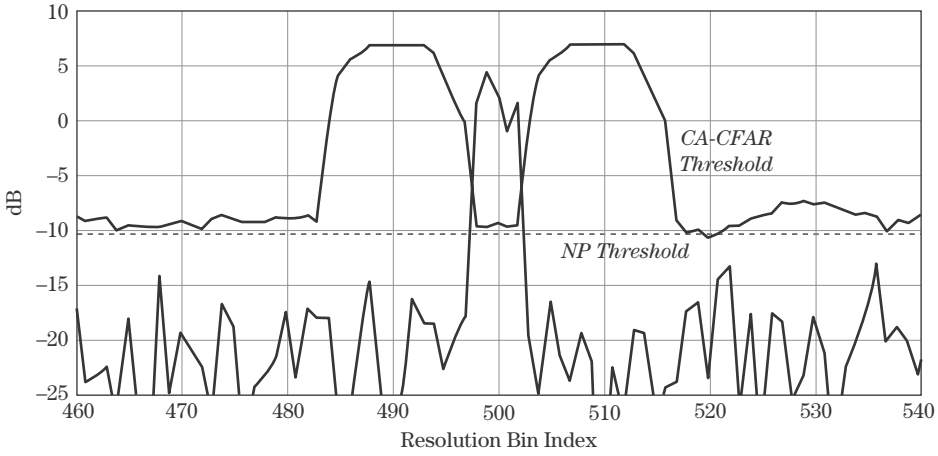

FIGURE 16-10 ■ Adding guard cells to the CA-CFAR ($N = 20$, $N_G = 16$) produces an adaptive threshold that detects the extended target.

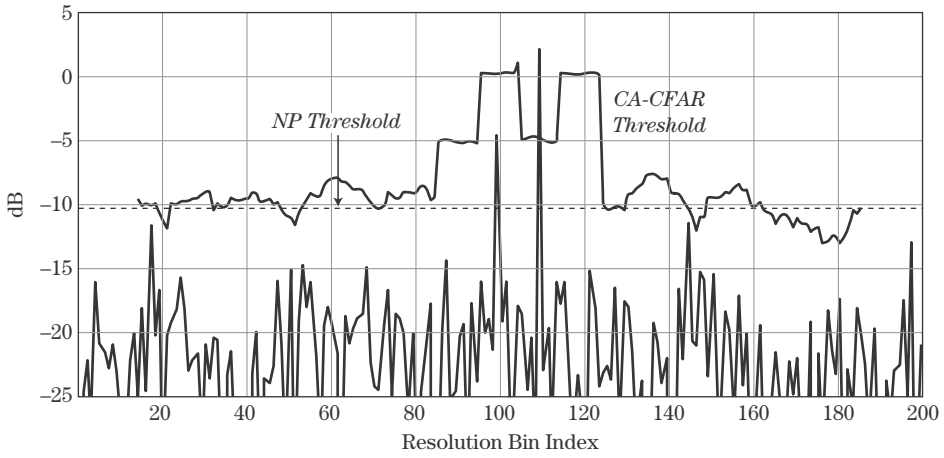

FIGURE 16-11 ■ Mutual target masking can occur for closely-spaced targets: two Rayleigh distributed point targets separated by 10 resolution bins with average $SINR = 20$ dB. CA-CFAR has $N = 20$ and $N_G = 16$.

on the right is not masked. The bias associated with the smaller target was not sufficient to mask the presence of the larger target.

Target masking is statistical in nature as observed in the previous example, where one target masked the presence of the other but the converse did not occur. Masking is a function of the reference window size, the desired P_{FA}, the number of interfering targets, and the ratio of the interfering target's power to that of the target in the CUT.

Gandhi and Kassam [7] derive an expression for the P_D associated with a CA-CFAR with target returns present in the reference window. The target returns are assumed to be Rayleigh distributed and independent. Consider a target in the CUT with an SINR denoted $SINR_{CUT}$ and M interfering targets, each with SINR denoted $SINR_{IT}$. The P_D achieved with a CA-CFAR in the presence of M interfering targets is [7]

$$P_{D_M} = \left[1 + \frac{\alpha'_{CA}(1 + SINR_{IT})}{1 + SINR_{CUT}}\right]^{-M} \left[1 + \frac{\alpha'_{CA}}{1 + SINR_{CUT}}\right]^{M-N} \tag{16.33}$$

where α'_{CA} is defined in equation (16.25).

A plot of P_D as a function of M for a $P_{FA} = 10^{-6}$, $SINR_{CUT} = 20$ dB, and $SINR_{IT} = \{5, 10, 15, 20 \text{ dB}\}$ is provided in Figure 16-12. P_D is reduced from 82% for $M = 0$ to 42% for $M = 1$ when $SINR_{CUT} = SINR_{IT} = 20$ dB.

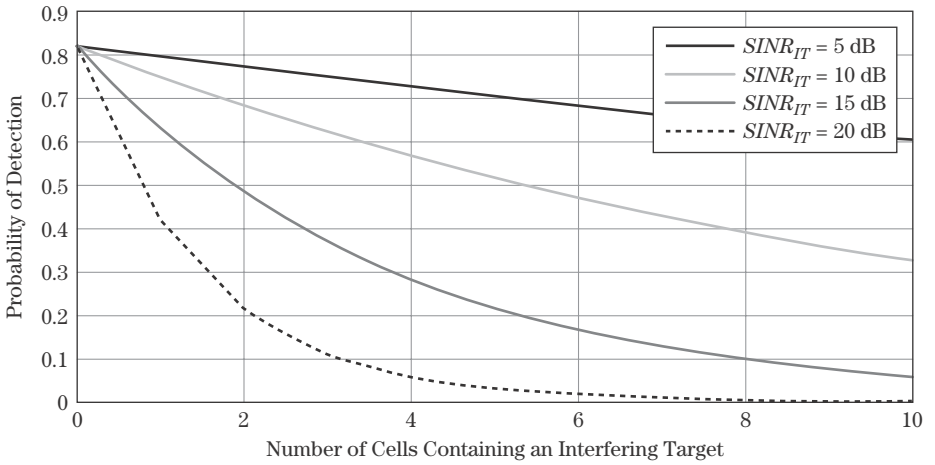

FIGURE 16-12 ■ For a CA-CFAR, P_D as a function of the number of targets in the reference window. Simulation parameters include $SINR_{CUT} = 20$ dB, $N = 20$ cells, and $P_{FA} = 10^{-6}$.

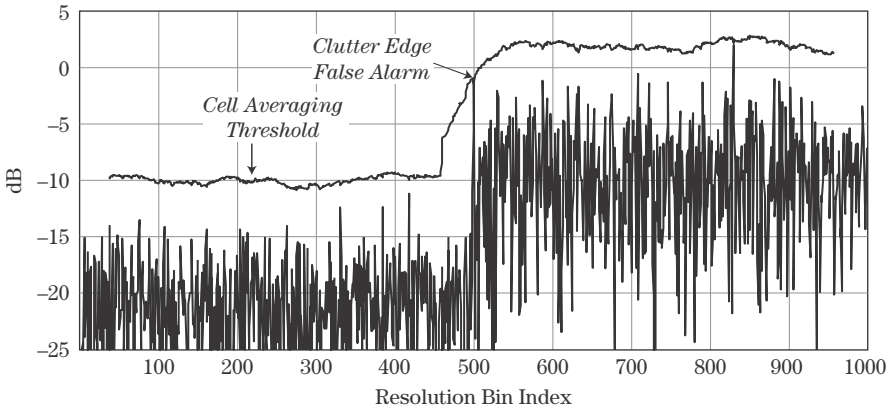

FIGURE 16-13 ■ The CA-CFAR threshold generates a clutter edge false alarm at the clutter boundary.

16.5.4.2 Clutter Boundaries

Significant and abrupt changes in terrain reflectivity impact both the false alarm rate and target masking. Abrupt changes in terrain reflectivity are termed *clutter boundaries* and are indicative of a change in terrain type or grazing angle. A data window containing a clutter boundary is illustrated in Figure 16-13. The presence of a clutter boundary has two primary effects on CFAR performance. The first is a reduction in P_D for targets positioned on the low reflectivity side of the clutter boundary. This condition is termed clutter edge masking. The second is an increase in the number of false alarms near the clutter boundary. A clutter edge false alarm is illustrated in Figure 16-13. The lower reflectivity region biases the threshold down as the CFAR window passes over the clutter boundary resulting in a false alarm.

Gandhi and Kassam [7] derive bounds on detection performance for a CA-CFAR in proximity to a clutter boundary. Consider a reference window that contains a clutter boundary. The clutter returns to the left of the clutter boundary are defined to have an average power level of $\sigma_{C_L}^2$, and clutter returns to the right of the clutter boundary are larger in terms of reflectivity and are defined to have an average power level of $\sigma_{C_H}^2$ where $\sigma_{C_L}^2 < \sigma_{C_H}^2$. Target and clutter returns are immersed in receiver noise with noise power defined by σ_n^2. For a target located in the lower clutter reflectivity region, P_D may be expressed as [7]

$$P_{D_{CB}} = \left[1 + \frac{\alpha'_{CA}\dfrac{\sigma_{C_H}^2 - \sigma_{C_L}^2}{\sigma_n^2 + \sigma_{C_L}^2}}{1 + \dfrac{\sigma_t^2}{\sigma_n^2 + \sigma_{C_L}^2}}\right]^{-M_H} \left[1 + \frac{\alpha'_{CA}}{1 + \dfrac{\sigma_t^2}{\sigma_n^2 + \sigma_{C_L}^2}}\right]^{M_H - N} \tag{16.34}$$

where M_H is the number of samples in the leading window that lie in the higher reflectivity region, and σ_t^2 is the power in the target return. The quantity $\sigma_t^2/(\sigma_n^2 + \sigma_{C_L}^2)$ represents the target's SINR in the lower reflectivity region, and $(\sigma_{C_H}^2 - \sigma_{C_L}^2)/(\sigma_n^2 + \sigma_{C_L}^2)$ represents the differential clutter reflectivity between the two regions normalized by the total interference in the lower reflectivity region. For purposes of notation, define $\Delta C = (\sigma_{C_H}^2 - \sigma_{C_L}^2)/(\sigma_n^2 + \sigma_{C_L}^2)$. Using (16.34), P_D is plotted in Figure 16-14 as a function of M_H for four values of ΔC (5, 10, 15, and 20 dB) and with $SINR = 20$ dB, $N = 20$, and $P_{FA} = 10^{-4}$. As observed, the potential for a clutter boundary to mask a nearby target is a function of both the number of higher reflectivity returns present in the reference window and the difference in reflectivity between the two regions.

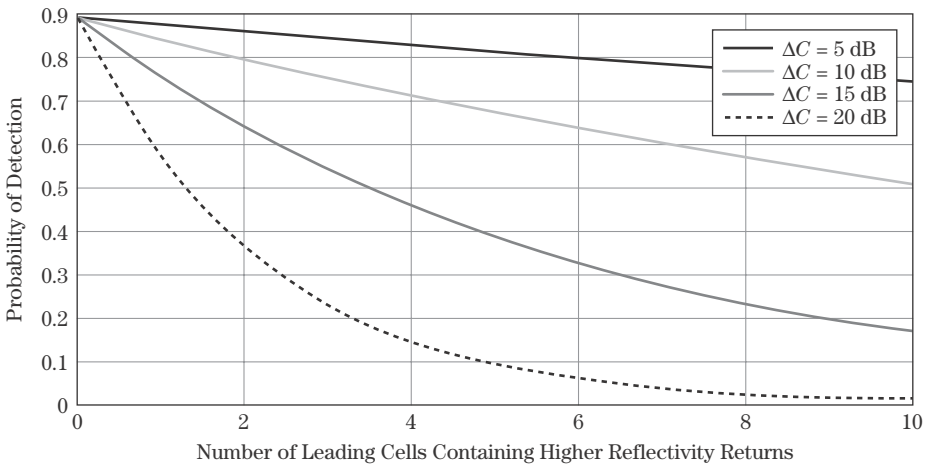

FIGURE 16-14 ■ For a CA-CFAR, P_D as a function of the number of returns associated with the higher reflectivity region. Simulation parameters include $SINR = 20$ dB, $N = 20$, and $P_{FA} = 10^{-4}$.

Clutter boundaries also influence the likelihood of a false alarm. Whether the boundary causes an increase or decrease in the P_{FA} depends on the location of the CUT. If the CUT is located in the lower reflectivity region, a reduction in the false alarm rate is observed as samples from the higher reflectivity region fall in the leading window and bias the threshold higher. An expression for P_{FA} when the CUT is positioned in the lower reflectivity region is [7]

$$P_{FA_{CB-low}} = \left[1 + \left(1 + \frac{\sigma_{C_H}^2 - \sigma_{C_L}^2}{\sigma_{C_L}^2 + \sigma_n^2}\right)\alpha'_{CA}\right]^{-M_H} [1 + \alpha'_{CA}]^{M_H - N} \tag{16.35}$$

where M_H is the number of samples in the higher reflectivity region contained within the leading reference window. If the CUT is located in the higher reflectivity region, a higher false alarm rate is observed provided the lagging window contains some samples associated with the lower reflectivity region. The expression for P_{FA} when the CUT is positioned in the higher reflectivity region is [7]

$$P_{FA_{CB-high}} = [1 + \alpha'_{CA}]^{-M_H} \left[1 + \frac{\alpha'_{CA}}{\left(1 + \frac{\sigma_{C_H}^2 - \sigma_{C_L}^2}{\sigma_{C_L}^2 + \sigma_n^2}\right)}\right]^{M_H - N} \tag{16.36}$$

The two expressions for P_{FA} in equations (16.35) and (16.36) are plotted in Figures 16-15 and 16-16, respectively, for $N = 20$ and $P_{FA} = 10^{-3}$. P_{FA} is maximum when the CUT lies in the higher reflectivity region, and the lagging reference window contains returns exclusive to the lower reflectivity region.

16.6 ROBUST CFARs

As previously discussed, a CA-CFAR's performance may degrade significantly in the presence of interfering targets and clutter boundaries. Since the introduction of the CA-CFAR in 1968, researchers have developed alternative CFAR algorithms that are designed to achieve good performance under specific heterogeneous conditions. A level of robustness is achieved at the expense of increased CFAR loss, additional complexity, higher

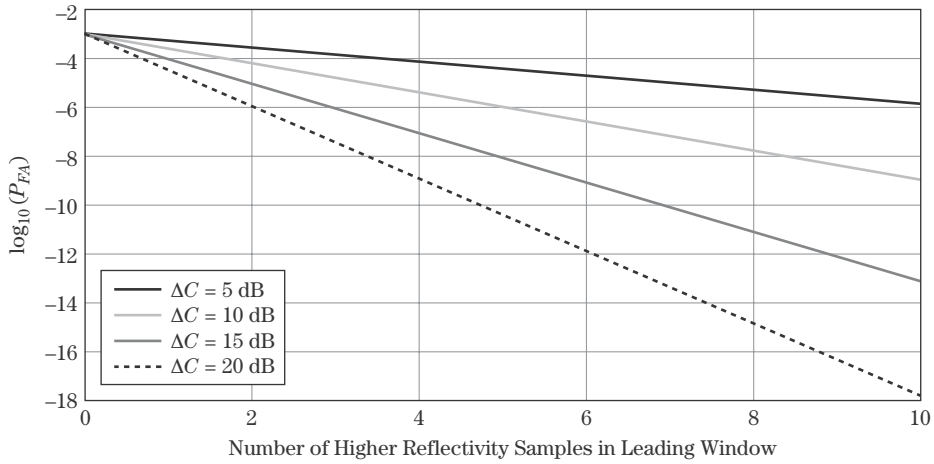

FIGURE 16-15 ■ For a CA-CFAR, P_{FA} as a function of the number of clutter cells associated with the higher reflectivity region when the cell-under-test (CUT) is located in the lower reflectivity region. Simulation parameters include $SINR = 20$ dB, $N = 20$, and $P_{FA} = 10^{-3}$.

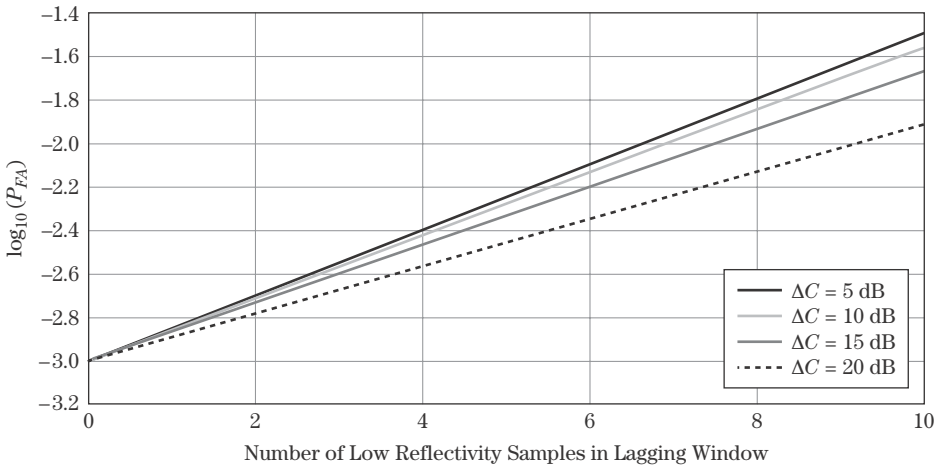

FIGURE 16-16 ■ For a CA-CFAR, P_{FA} as a function of the number of clutter cells associated with the lower reflectivity region when the CUT is located in the higher reflectivity region. Simulation parameters include $SINR = 20$ dB, $N = 20$, and $P_{FA} = 10^{-3}$.

computational cost, and CFAR constants that require iterative solutions. In general, robust CFAR algorithms require the user to possess some a priori knowledge about the target/clutter environment. For example, some algorithms require the user to define, a priori, the number of targets that may be present in the reference window and to use the number as an input to the algorithm to suppress mutual target masking.

Some of the more common CFARs include greatest-of CA-CFAR (GOCA-CFAR), smallest-of CA-CFAR (SOCA-CFAR), trimmed mean (TM) or censored (CS) CFAR, and order statistics (OS) CFAR. GOCA-CFAR is designed to minimize the number of clutter edge false alarms. SOCA-CFAR, TM-CFAR or CS-CFAR, and OS-CFARs are designed to suppress mutual target masking. The architecture and performance of each algorithm is examined in the following sections.

16.6.1 Greatest-of CA-CFAR

Hansen and Sawyers [5] developed the "greatest-of" CA-CFAR to reduce clutter edge false alarms. Clutter edge false alarms are suppressed by computing the average interference

power in the lagging and leading windows separately and selecting the larger of the two sample means as the CFAR statistic. Mathematically, the GOCA-CFAR may be expressed as

$$\hat{g}_{GO} = \max(\hat{f}_{GO,\,lag},\, \hat{f}_{GO,\,lead}) \tag{16.37}$$

where

$$\hat{f}_{GO,\,lag} = \sum_{i=1}^{N/2} z_i \tag{16.38}$$

and

$$\hat{f}_{GO,\,lead} = \sum_{i=N/2+1}^{N} z_i \tag{16.39}$$

Note that the $1/2N$ scale factor needed to compute the sample mean is accounted for in the CFAR constant. In a homogenous interference environment, the average P_D associated with a GOCA-CFAR [5–7] is defined by

$$P_{D_{GO}} = 2\left\{\left[1 + \frac{\alpha_{GO}}{1 + SINR}\right]^{-\frac{N}{2}} - \left[2 + \frac{\alpha_{GO}}{1 + SINR}\right]^{-\frac{N}{2}} \times \sum_{k=0}^{N/2-1} \binom{\frac{N}{2} - 1 + k}{k} \left[2 + \frac{\alpha_{GO}}{1 + SINR}\right]^{-k}\right\} \tag{16.40}$$

and the average P_{FA} is found by setting $SINR = 0$, yielding

$$P_{FA_{GO}} = 2\left\{[1 + \alpha_{GO}]^{-\frac{N}{2}} - [2 + \alpha_{GO}]^{-\frac{N}{2}} \sum_{k=0}^{N/2-1} \binom{\frac{N}{2} - 1 + k}{k} [2 + \alpha_{GO}]^{-k}\right\} \tag{16.41}$$

The binomial coefficients, denoted $\binom{m}{n}$ where m and n are integers, are defined by

$$\binom{m}{n} = \frac{m!}{(m-n)!n!} \tag{16.42}$$

and are found in many of the subsequent expressions for P_D and P_{FA}.

The GOCA-CFAR threshold is defined as the product of the statistic in equation (16.37) and the CFAR constant embedded in equation (16.41). Solving for the CFAR constant in (16.41) is more difficult than in the case of a CA-CFAR and requires an iterative solution. A complex relationship between P_{FA} and α is inherent in most robust CFAR algorithms.

CFAR loss is an important performance metric and is used in comparing the strength of different CFAR algorithms. Hansen and Sawyers [5] show that the additional CFAR loss associated with a GOCA-CFAR is ≤ 0.3 dB. This additional loss is defined relative to a CA-CFAR with an equivalent length reference window. The relationship holds even for small reference window sizes (e.g., $N = 4$). The additional CFAR loss typically ranges from 0.1 to 0.3 dB. Figure 16-17 contains a plot of the ROC associated with a CA-CFAR and a GOCA-CFAR with $N = 16$ and $P_{FA} = 10^{-6}$. As expected, the ROC associated with

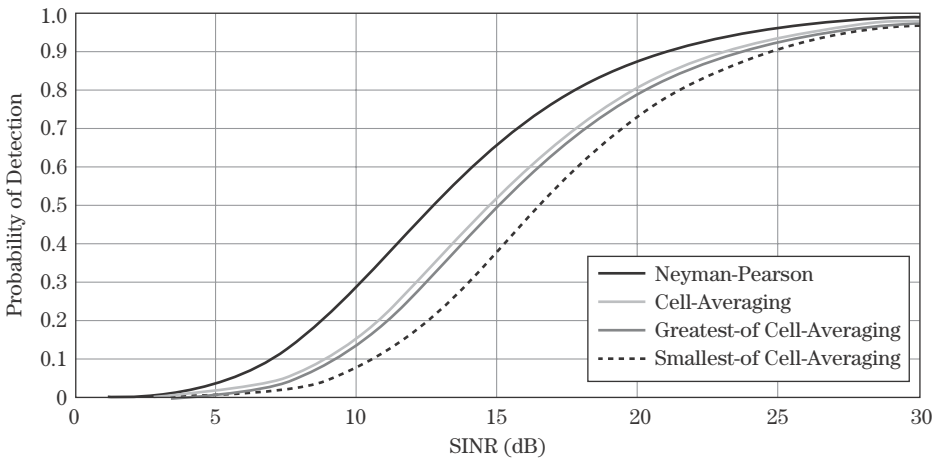

FIGURE 16-17 ■ ROC for an NP detector and three CFARs – CA, GO, and SO with $N = 16$ and $P_{FA} = 10^{-6}$.

the GOCA-CFAR appears to the right of the CA-CFAR. The larger CFAR loss is due to the fact that fewer samples are used in computing the GOCA-CFAR statistic. Table 16-1 contains a list of CFAR loss values recorded at the 90% P_D level for both the CA and GOCA-CFARs. The losses are defined for selected values of P_{FA} and N. Note that the difference between the CA and GOCA-CFAR is less than or equal to 0.3 dB.

A GOCA-CFAR reduces clutter edge false alarms by biasing the threshold above that of the CA-CFAR. The threshold tends to track the higher reflectivity region. Figure 16-18 contains simulated Rayleigh distributed interference for two clutter regions where the reflectivity between the two regions differs by 20 dB. The reference window is sized for $N = 40$, and the desired P_{FA} equals 10^{-3}. Superimposed on the plot are the CA and GOCA thresholds. The GOCA threshold tends to ride above the CA threshold as the CFAR window passes over the clutter boundary. In this particular data set, a false alarm is not observed; however, the GOCA-CFAR, with the higher threshold, is less susceptible to false alarms within the transition region. Gandhi and Kassam [7] provide an expression for a GOCA-CFAR's P_{FA} when a clutter boundary is present in the reference window.

GOCA-CFAR, with its ability to suppress clutter edge false alarms, exhibits degraded performance in the presence of interfering targets. Interfering targets capture the greatest-of logic and bias the CFAR threshold. Furthermore, the bias is greater relative to a

TABLE 16-1 ■ The CFAR Loss Associated with a CA-CFAR, GOCA-CFAR, and SOCA-CFAR

		CFAR Loss (dB)		
N	P_{FA}	CA-CFAR	GOCA-CFAR	SOCA-CFAR
8	10^{-4}	2.7	3.0	5.3
16	10^{-4}	1.3	1.5	2.3
24	10^{-4}	0.9	1.0	1.5
32	10^{-4}	0.6	0.8	1.0
8	10^{-6}	4.3	4.6	8.9
16	10^{-6}	2.0	2.2	3.8
24	10^{-6}	1.3	1.5	2.3
32	10^{-6}	1.0	1.1	1.7

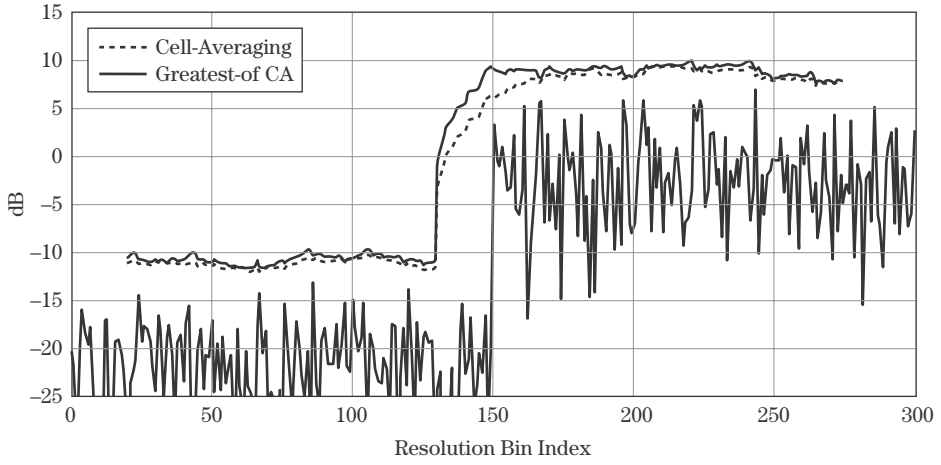

FIGURE 16-18 ■ The Greatest-Of CA-CFAR threshold is higher than a simple CA-CFAR threshold at a clutter boundary. The higher threshold reduces clutter edge false alarms.

CA-CFAR because the effective size of the reference window is reduced by a factor of 2. The reduction in the size of the reference window occurs because the estimate of the interference is computed separately for the leading and lagging windows and only one estimate is used to set the threshold. Weiss [6] has examined CFAR performance for the case of a single, Swerling 1 target located in either the leading or lagging window and has provided bounds on P_D for both CA and GOCA-CFARs. The bounds are defined for the limiting cases where $SINR_{CUT}$ and $SINR_{IT}$ tend toward infinity and the ratio $SINR_{IT}/SINR_{CUT}$ is a constant. The bound on P_D for GOCA is

$$\lim_{SINR_{CUT},\, SINR_{IT}\to\infty} P_{D_{GO}} = \left[1 + \frac{SINR_{IT}}{SINR_{CUT}}\alpha_{GO}\right]^{-1} \tag{16.43}$$

and for CA is

$$\lim_{SINR_{CUT},\, SINR_{IT}\to\infty} P_{D_{CA}} = \left[1 + \frac{SINR_{IT}}{SINR_{CUT}}\alpha'_{CA}\right]^{-1} \tag{16.44}$$

Note that the GOCA-CFAR constant, α_{GO}, in equation (16.43) is larger than the CA-CFAR constant, α'_{CA}, in equation (16.44) [6]. Given an interfering target, the larger GOCA-CFAR constant produces a lower P_D compared with a CA-CFAR.

Figure 16-19 contains a plot comparing the detection performance of a CA-CFAR and GOCA-CFAR, based on equations (16.43) and (16.44), when a single interferer lies within the reference window. For this example, the simulation parameters are $N = 20$ and $P_{FA} = 10^{-4}$. The abscissa in Figure 16-19 represents the ratio of the power in the interfering target to that in the target located in the CUT. With an interfering target 1/10th as large as the target in the CUT, the CA-CFAR achieves a $P_D \approx 95\%$, whereas the GOCA-CFAR achieves a $P_D \approx 90\%$.

As a final comment, when applying the bounds in equations (16.43) and (16.44), care must be taken to recognize the limiting conditions placed on SINR. Also, note that an exact expression for P_D for a CA-CFAR with interfering targets is provided in (16.33).

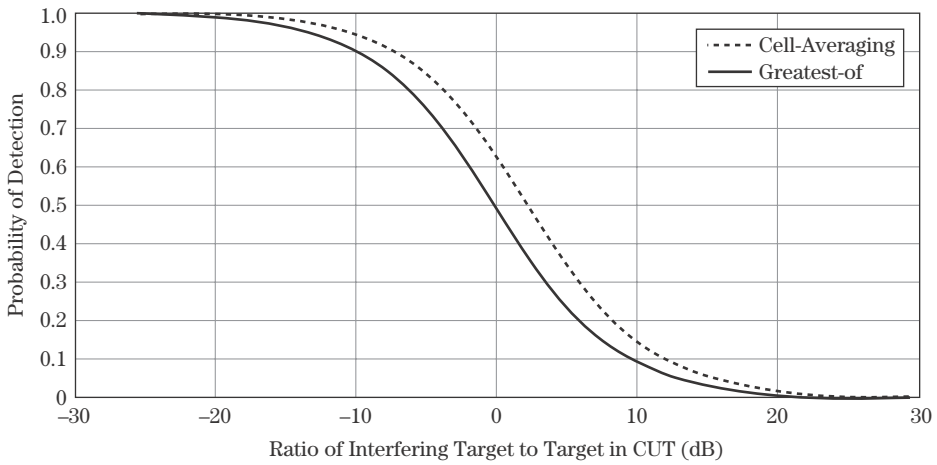

FIGURE 16-19 ■ Weiss' performance bounds for a CA and GOCA-CFAR in the presence of an interfering target. The CFAR parameters are $N = 20$ and $P_{FA} = 10^{-4}$.

16.6.2 Suppression of Mutual Target Masking

Several CFAR algorithms have been designed to address mutual target masking: SOCA-CFAR, CS-CFAR or TM-CFAR, and OS-CFAR. These algorithms are described in the following sections.

16.6.2.1 Smallest-of CA-CFAR

Trunk [8] proposed a smallest-of CA-CFAR to address mutual target masking. The SOCA-CFAR estimates the interference power in the lagging and leading reference windows and selects the smaller of the two estimates as the CFAR statistic. The smaller of the two estimates is selected to suppress interfering targets that may reside in either the leading or lagging window but not targets present simultaneously in both windows. The SOCA-CFAR statistic is defined as

$$\hat{g}_{SO} = \min(\hat{f}_{SO,lag}, \hat{f}_{SO,lead}) \tag{16.45}$$

where

$$\hat{f}_{SO,lag} = \sum_{i=1}^{N/2} z_i \tag{16.46}$$

and

$$\hat{f}_{SO,lead} = \sum_{i=N/2+1}^{N} z_i \tag{16.47}$$

The SO threshold is defined as

$$T_{SO} = \alpha_{SO} \hat{g}_{SO} \tag{16.48}$$

In a homogenous interference environment, the average P_D for a SOCA-CFAR [6] is defined as

$$P_{D_{SO}} = 2\left[2 + \frac{\alpha_{SO}}{1 + SINR}\right]^{-\frac{N}{2}} \sum_{k=0}^{N/2-1} \binom{\frac{N}{2} - 1 + k}{k} \left[2 + \frac{\alpha_{SO}}{1 + SINR}\right]^{-k} \tag{16.49}$$

and the average P_{FA} is found by setting $SINR = 0$, giving

$$P_{FA_{SO}} = 2[2 + \alpha_{SO}]^{-\frac{N}{2}} \sum_{k=0}^{N/2-1} \binom{\frac{N}{2} - 1 + k}{k} [2 + \alpha_{SO}]^{-k} \tag{16.50}$$

SOCA-CFAR exhibits two properties that limit its practical application. First, a SOCA-CFAR's ability to suppress mutual target masking is limited to cases where the interfering targets are restricted to either the leading or lagging windows. Performance is severely degraded when interfering targets are present in both windows. Second, a SOCA-CFAR exhibits a relatively large CFAR loss when compared with other CFAR algorithms with equivalent size reference windows. The SOCA CFAR loss is observed in Figure 16-17. At 90% P_D, the CFAR loss associated with the SOCA-CFAR is 1.8 dB greater than a CA-CFAR and 1.6 dB greater than a GOCA-CFAR. The difference in CFAR loss between a CA-CFAR and a SOCA-CFAR varies depending on the value of N and P_{FA} as illustrated in Table 16-1. For these cases, the difference in CFAR loss ranges from 0.4 dB to 4.6 dB.

16.6.2.2 Trimmed Mean or Censored CFAR

Rickard and Dillard [9] and Ritcey [10] define a censored CFAR, which rank orders the measured samples in the reference window and discards the largest N_C samples prior to computing the CFAR statistic. The assertion is that the largest N_C samples may contain returns from interfering targets and therefore should not be used in estimating the CFAR statistic. The CFAR statistic is an estimate of the average power in the remaining reference cells. The CS-CFAR is capable of removing N_C interfering targets from the reference window. The user is required to assume, a priori, the maximum number of targets that may be present in the reference window and to use this number to set N_C. For a fixed reference window size, increasing N_C increases the CFAR loss as the number of samples used in estimating the CFAR statistic decreases; therefore, N_C should be selected taking into account the number of potential interfering targets and the CFAR loss incurred.

Gandhi and Kassam [7] present a more general form of the CS-CFAR algorithm termed a trimmed mean CFAR, which discards the N_{T_L} largest and N_{T_S} smallest samples. The TM-CFAR is a rank-ordered approach that computes the mean interference power from a subset of samples. A TM-CFAR may be tailored to address different interference environments by adjusting the two parameters, N_{T_S} and N_{T_L}, for specific conditions. It can shown that an OS-CFAR and CA-CFAR are special cases of the TM-CFAR with $(N_{T_S}, N_{T_L}) = (k - 1, N - k)$ and $(0, 0)$, respectively. An OS-CFAR and the variable k are defined in the next section.

In general, N_{T_L} is selected to remove interfering targets, and N_{T_S} is selected to suppress clutter edge false alarms. As in the case of a CS-CFAR, N_{T_L} is selected to match an a priori estimate of the maximum number of interfering targets in the reference window. If a goal is to minimize clutter edge false alarms, then N_{T_S} should be selected as a significant percentage of N. To address both clutter edge false alarms and target masking, Gandhi [7] suggests that for $N = 24$, let $N_{T_S} = 18$ to 20 and $N_{T_L} = 1$ to 3.

Expressions for the average P_D and P_{FA} for the both the TM-CFAR and CS-CFARs are given by

$$P_{D_{TM}} = \prod_{i=1}^{N-N_{T_S}-N_{T_L}} \gamma_i(\nu)\Big|_{\nu = \frac{\alpha_{TM}}{1+SINR}} \tag{16.51}$$

and

$$P_{FA_{TM}} = \prod_{i=1}^{N-N_{T_S}-N_{T_L}} \gamma_i(\nu)\Big|_{\nu=\alpha_{TM}} \tag{16.52}$$

where

$$\gamma_1 = \frac{N!}{N_{T_S}!(N-N_{T_S}-1)!(N-N_{T_S}-N_{T_L})} \sum_{k=0}^{N_L} \frac{\binom{N_{T_S}}{k}(-1)^{N_{T_S}-k}}{\frac{N-k}{N-N_{T_S}-N_{T_L}}+\nu} \tag{16.53}$$

and

$$\gamma_i = \frac{\frac{N-N_{T_S}-i+1}{N-N_{T_S}-N_{T_L}-i+1}}{\frac{N-N_{T_S}-i+1}{N-N_{T_S}-N_{T_L}-i+1}+\nu} \quad i=2,\ldots,(N-N_{T_S}-N_{T_L}) \tag{16.54}$$

The CFAR constant in equation (16.52) contains the scale factor used in computing the sample mean. Note that the CS-CFAR is a special case of the TM-CFAR with $N_{T_S}=0$ and $N_{T_L}=N_C$.

16.6.2.3 Order Statistics CFAR

Rohling [11,12] defines an order statistics CFAR that is designed to suppress target masking. The OS-CFAR rank orders the N samples in the CFAR reference window and selects the k-th sample as the CFAR statistic. The CFAR is thus capable of rejecting $N-k$ interfering targets. In addition, an OS-CFAR is capable of suppressing clutter edge false alarms provided $k > N/2$ [7,11].

Gandhi and Kassam [7] provide the following expressions for the average P_D and P_{FA}:

$$P_{D_{OS}} = \prod_{i=0}^{k-1} \frac{N-i}{N-i+\frac{\alpha_{OS}}{1+SINR}} \tag{16.55}$$

and

$$P_{FA_{OS}} = \prod_{i=0}^{k-1} \frac{N-i}{N-i+\alpha_{OS}} \tag{16.56}$$

where α_{OS} is the OS-CFAR constant. An equivalent expression for the average P_{FA} is [11]

$$P_{FA_{OS}} = k\binom{N}{k}\frac{(k-1)!(\alpha_{OS}+N-k)!}{(\alpha_{OS}+N)!} \tag{16.57}$$

Rohling [11] examines the CFAR loss associated with an OS-CFAR and shows that it exhibits a relatively broad minimum as a function of k. To achieve a CFAR loss near the minimum, a reasonable value of k is $3N/4$. This value of k also supports the suppression of $N/4$ interfering targets.

For a given value of N, an OS-CFAR exhibits a CFAR loss greater than that exhibited by a CA-CFAR. With its ability to suppress mutual target masking, the length of an OS-CFAR's reference window may be extended to reduce the CFAR loss. The longer reference window may contain additional interfering targets, but the algorithm is designed to suppress them. From a CFAR loss perspective, similar detection performance may be achieved in a homogenous interference environment using a CA-CFAR with $N=16$ or an OS-CFAR with $N=24$ [11].

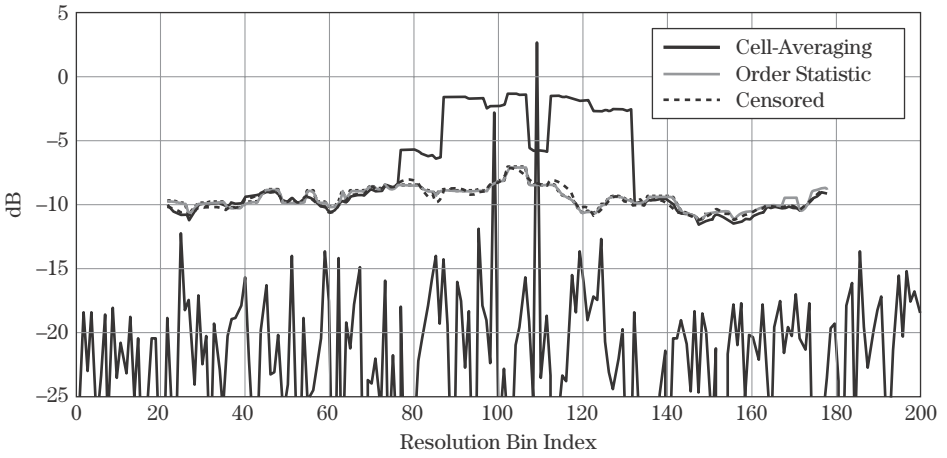

FIGURE 16-20 ■ The Order Statistic (OS), and Censored CS(2) CFARs mitigate mutual target masking while the CA-CFAR misses one target.

An OS-CFAR may also be used to address self-target masking. An OS-CFAR eliminates the need for guard cells (i.e., $N_G = 0$) provided the total number of reference cells containing target returns is less than $N - k$.

The discussion to this point has been limited to square law detectors. However, for the case of an OS-CFAR a simple expression does exists that relates the CFAR constants associated with a linear and square law detector. The two OS-CFAR constants are related via [11]

$$\alpha_{OS_{\text{linear}}} = \sqrt{\alpha_{OS_{\text{square law}}}} \tag{16.58}$$

This relationship does not apply to other CFAR algorithms (e.g., CA-CFAR).

16.6.2.4 CS- and OS-CFAR Numerical Example

The ability of a CS-CFAR and OS-CFAR to mitigate target masking is illustrated in the following example. Consider two Swerling 1 targets embedded in Rayleigh distributed interference with an average $SINR = 20$ dB. Figure 16-20 contains a plot of the CA-, CS-, and OS-CFAR thresholds derived from the simulated returns. The detectors are designed to achieve a $P_{FA} = 10^{-4}$. The reference window consists of 40 cells. The CS-CFAR discards the largest two samples (denoted CS(2)), and the OS-CFAR uses the 30th sample to compute the CFAR statistic. In this example, both the CS- and OS-CFARs detect the two targets, whereas the CA-CFAR detects only the larger target. The OS-CFAR is capable of suppressing 10 interfering targets, and the CS-CFAR is capable of suppressing two interfering targets.

16.6.3 Combining GO with CS or OS

Both order statistics and censored CFARs are designed to address mutual target masking. Each algorithm rank orders the samples in the reference window and excludes some number of the largest samples when computing the interference statistic. In suppressing some of the larger returns, these CFAR techniques are susceptible to clutter edge false alarms. Several authors [17–20] have examined combining greatest-of with OS- and CS-CFARs to provide robustness in the presence of multiple targets and clutter boundaries. The first step is to apply either an OS- or CS-CFAR to the leading and lagging reference

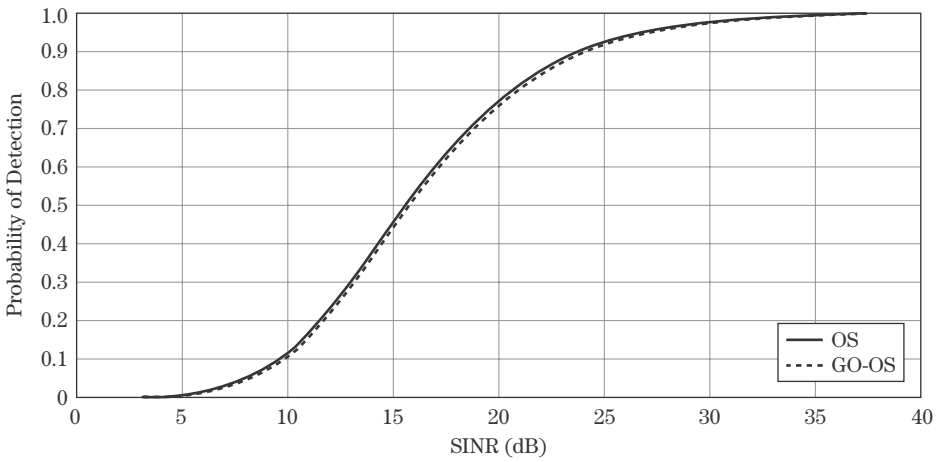

FIGURE 16-21 ■ ROC for OS and GO-OS CFARs with $N = 16$ and $P_{FA} = 10^{-6}$.

windows separately to address mutual target masking. Next, the larger of the two statistics is then selected to suppress clutter edge false alarms. The acronyms GO-OS and GO-CS CFAR are used to denote greatest-of order statistics and greatest-of censored CFAR, respectively.

Elias-Fuste [17] provides expressions for P_D and P_{FA} when applying GO-OS CFAR. The average P_D is defined by

$$P_{D_{GO-OS}} = 2k^2 \binom{N/2}{k}^2 \sum_{j=0}^{N/2-k} \sum_{i=0}^{N/2-k} \binom{N/2-k}{j} \binom{N/2-k}{i} \times \cdots$$
$$\cdots \frac{(-1)^{N-2k-j-i}}{N/2-i} \frac{\Gamma(N-j-i)\Gamma(\alpha_{GO-OS}/(1+SINR)+1)}{\Gamma(N-j-i+\alpha_{GO-OS}/(1+SINR)+N/2+1)} \tag{16.59}$$

and the average P_{FA} is defined by

$$P_{FA_{GO-OS}} = 2k^2 \binom{N/2}{k}^2 \sum_{j=0}^{N/2-k} \sum_{i=0}^{N/2-k} \binom{N/2-k}{j} \binom{N/2-k}{i} \times \cdots$$
$$\cdots \frac{(-1)^{N-2k-j-i}}{N/2-i} \frac{\Gamma(N-j-i)\Gamma(\alpha_{GO-OS}+1)}{\Gamma(N-j-i+\alpha_{GO-OS}+N/2+1)} \tag{16.60}$$

where $\Gamma(\,)$ is the Gamma function. Figure 16-21 contains a plot comparing the ROCs for an OS- and GO-OS CFAR. The reference window is length 16, and detector is designed to exhibit a P_{FA} equal to 10^{-6}. The additional CFAR loss associated with combining GO and OS is only a few tenths of a dB.

16.7 ALGORITHM COMPARISON

The selection of a CFAR processor and its parameters is highly dependent on the heterogeneity of the interference environment. In a homogeneous environment, the cell averaging CFAR [6] maximizes P_D for a given reference window size, and its performance approaches that of the Neyman-Pearson detector as the window size is increased. However,

TABLE 16-2 ■ CFAR Algorithms and the Environments in which They Were Designed to Operate

	Environment			
CFAR	Homogeneous	Interfering Targets	Clutter Boundaries	Interfering Targets and Clutter Boundaries
CA	X			
GOCA			X	
SOCA		X		
CS		X		
TM		X	X	X
OS		X	X	X
GO-OS		X	X	X
GO-CS		X	X	X

as previously discussed, heterogeneous interference significantly degrades the P_D and P_{FA} performance of a CA-CFAR. To operate in heterogeneous environments, "robust" CFARs have been developed to address specific operational conditions. In many cases, a CFAR is designed to address either target masking or clutter edge false alarms. The burden is on the user to possess a priori knowledge of the interference environment and to select the CFAR best tailored to that environment. Table 16-2 contains a list of CFAR algorithms and the interference environments in which they are designed to operate. Note that the SOCA-CFAR is capable of suppressing target masking only when the interferers fall in one of the two reference windows and not both.

When selecting a CFAR algorithm, the impact of CFAR loss on detection performance must be considered. To illustrate the point, consider the ROCs for five CFAR algorithms: CA, GOCA, SOCA, CS, and OS. The ROCs are plotted in Figure 16-22. Each detector is designed to achieve a P_{FA} equal to 10^{-6}. All reference windows are length 16, and the CS-CFAR discards the largest four samples. For the OS-CFAR, $k = 12$. The CFAR loss associated with the CA-CFAR is 2 dB at the 90% P_D mark. In comparison, the GOCA-CFAR exhibits 2.25 dB of loss, and the CS- and OS-CFARs exhibit approximately 2.9 dB of loss. The CS-CFAR ROC appears to left of the OS-CFAR ROC, and the difference in CFAR loss between them is less than 0.05 dB. As with any of the CFAR algorithms,

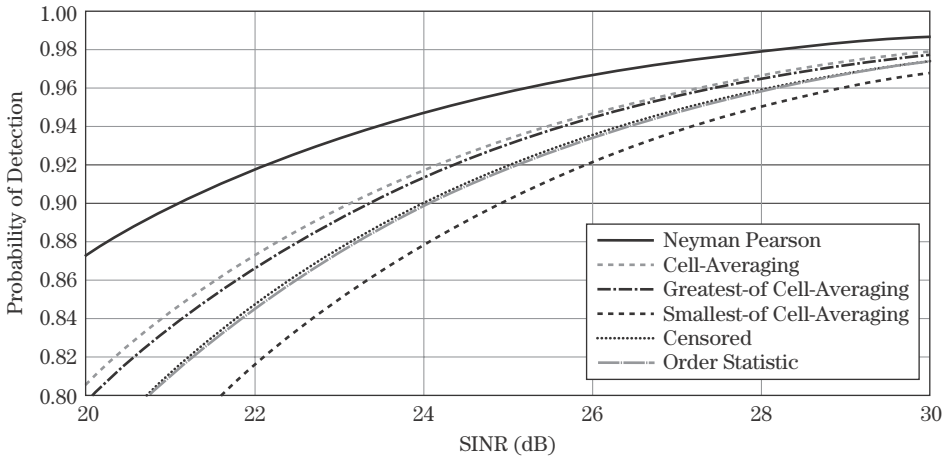

FIGURE 16-22 ■ ROCs for NP detector and CA, GOCA, SOCA, CS(4), and OS ($k = 3N/4$) CFARs with $N = 16$ and $P_{FA} = 10^{-6}$.

the size of the reference window can be increased to decrease the CFAR loss; however, the impact of heterogeneity and additional computations must also be considered when employing a larger window.

16.8 ADAPTIVE CFARs

The robust CFARs examined in the previous sections rely heavily on the user's a priori knowledge of the interference environment to select the most appropriate CFAR and its parameters. For example, when applying a censored CFAR, the number of cells to discard must be selected a priori. The number of cells is dependent on the user's knowledge or assumptions regarding the number of targets that might lie in the reference window. Since the mid 1980s, a number of algorithms have appeared in the literature that are designed to adaptively select CFAR parameters based on the measured data rather than on the user's assumptions regarding the environment. In this text, these algorithms are referred to as *adaptive* CFARs. One of the first adaptive algorithms to appear in the literature was the heterogeneous clutter estimating (HCE) CFAR developed by Finn [21]. The algorithm seeks to identify the location of the clutter boundary within the reference window and to use only samples associated with the same distribution as the CUT to compute the interference statistic. The HCE-CFAR is designed to address both clutter edge false alarms and target masking.

Adaptive CFARs offer significant P_D and P_{FA} performance advantages. The price for performance is a significant increase in the number of computations. Several adaptive CFARs appear in the literature [21–25]. The generalized censored mean level detector (GCMLD) [22] is an adaptive censored CFAR. The GCMLD estimates the number and location of interfering targets contained within the reference window and discards them prior to calculating the interference statistics. The greatest-of/smallest-of CFAR [25] is designed to estimate the location of a clutter boundary and is similar in its approach to the HCE-CFAR. Himonas and Barkat [25] have also combined the properties of the GO/SO and GCMLD into a single CFAR termed the generalized two-level censored mean level detector to address both target masking and clutter edge false alarms.

To illustrate the potential performance gains associated with an adaptive CFAR, consider the performance of a CA, CS, and GCMLD with two interfering targets located within the reference window. Figure 16-23 contains the ROC for a CA- and CS-CFAR

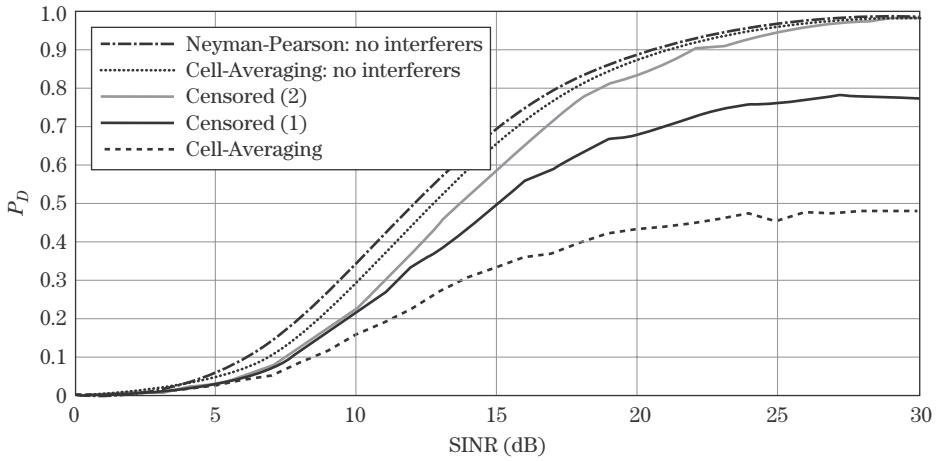

FIGURE 16-23 ROC for CA, CS(1), and CS(2) CFARs with two interferers in the reference window and $SINR = SINR_{IT}$.

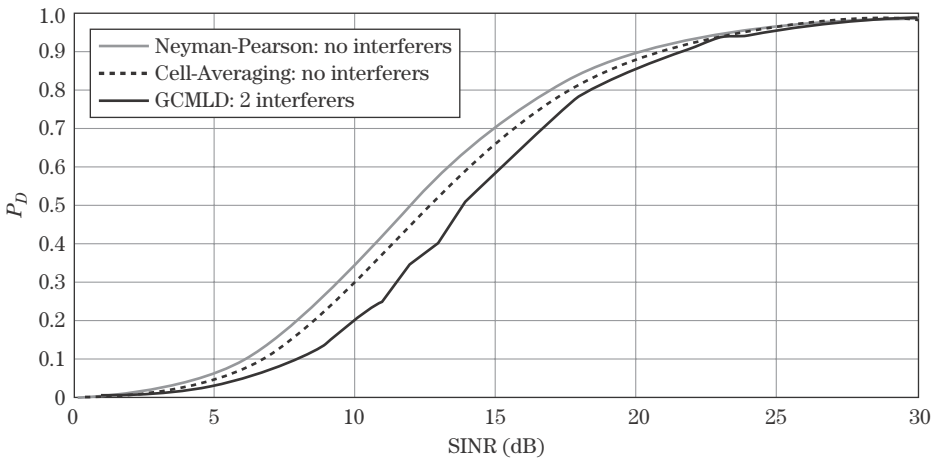

FIGURE 16-24 ■ ROC for an adaptive-censored (GCMLD) CFAR with two interferers in the reference window and $SINR = SINR_{IT}$ shows excellent performance without preselecting the number of samples to discard.

with two interfering targets and $SINR_{IT} = SINR_{CUT}$. The performance of an NP detector and CA-CFAR, with no interferers present, is also plotted as a reference. The CFARs are designed with $N = 30$ and $P_{FA} = 10^{-5}$. With two interferers, the CA-CFAR yields less than 50% P_D. The CS-CFAR, discarding the largest return (denoted CS(1)), yields less than 80% P_D. If the number of interfering targets was guessed correctly so that the largest two samples were discarded, then performance approaches that of a CA with no interferers. As expected, the CS(2)-CFAR exhibits some additional CFAR loss over the CA-CFAR with no interferers present.

The GCMLD operates on the measured data with no assumption regarding the number of targets in the reference window. It estimates the number of interferers from the measurements in the reference window. The performance of the GCMLD is illustrated in Figure 16-24 against the two interferers. The ROC for the GCMLD approaches that of the CS(2)-CFAR. The GCMLD and other adaptive CFARs hold promise for the future, provided that computational resources are available to support real-time implementation.

16.9 ADDITIONAL COMMENTS

16.9.1 Non-Rayleigh Backgrounds

The CFAR algorithms examined in this chapter are designed to operate in environments composed of Rayleigh distributed interference. However, some backgrounds (e.g., low grazing angle terrain, high-resolution imagery, reflections from the sea) are more accurately described using log normal, Weibull, or K distributions, which exhibit longer tails. These distributions are defined by both a scale and a shape parameter [26], which must be estimated to characterize the interference. CFAR algorithms have been designed for operation in these environments and are described in [26–31].

16.9.2 Clutter Map CFAR

The CFAR algorithms covered in this chapter use samples contained within a reference window to estimate the interference statistics. The reference window is moved in one or more dimensions, and the interference within the window is assumed to be relatively homogeneous. Clutter boundaries may exist, but large sections of the reference window

contain homogeneous interference. In environments where the interference is heterogeneous from resolution cell to resolution cell, a clutter map CFAR may be employed. A clutter map CFAR computes the interference statistics within a given resolution cell using samples collected temporally (e.g., scan to scan). Nitzberg and Levanon [32,33] provide a discussion of the implementation and performance of clutter map CFARs.

16.10 FURTHER READING

Survey papers that describe and compare the performance of different CFAR algorithms are worthy of further examination. Two excellent survey papers are Weiss [6], which examines CA-, GO-, and SO-CFARs, and Gandhi and Kassam [7], which examines CA-, GO-, SO-, OS-, and TM-CFARs. Levanon's *Radar Principles* [3] contains an excellent chapter on CFAR. The chapter includes a derivation of the CA- and OS-CFARs and introduces the reader to the concept of CFAR loss. Belcher, in *Radar Design Principles* by Nathason [34], provides a brief but comprehensive overview and comparison of a number of CFAR algorithms without delving into the complex derivations and equations. Richards' [13] recent text *Fundamentals of Radar Signal Processing* also provides an excellent and comprehensive chapter on CFAR, which includes derivations and performance metrics.

16.11 REFERENCES

[1] Hansen, V.G., and Ward, H.R., "Detection Performance of the Cell Averaging Log/CFAR Receiver," *IEEE Transactions on Aerospace and Electronic Systems,* vol. AES-8, no. 5, pp. 648–652, September 1972.

[2] Novak, L.M., "Radar Target Detection and Map-Matching Algorithm Studies," *IEEE Transactions on Aerospace and Electronic Systems*, vol. AES-16, no. 5, pp. 620–625, September 1980.

[3] Levanon, N., *Radar Principles*, John Wiley and Sons, New York, 1988.

[4] Finn, H.M., and Johnson, R.S., "Adaptive Detection Mode with Threshold Control as a Function of Spatially Sampled Clutter-Level Estimates," *RCA Review*, pp. 414–464, September 1968.

[5] Hansen, V.G., and Sawyers, J.H., "Detectability Loss Due to "Greatest of" Selection in a Cell-Averaging CFAR," *IEEE Transactions on Aerospace and Electronic Systems*, vol. AES-16, no. 1, pp. 115–118, January 1980.

[6] Weiss, M., "Analysis of Some Modified Cell-Averaging CFAR Processors in Multiple-Target Situations," *IEEE Transactions on Aerospace and Electronic Systems*, vol. AES-18, no. 1, pp. 102–114, January 1982.

[7] Gandhi, P.P., and Kassam, S.A., "Analysis of CFAR Processors in Nonhomogeneous Background," *IEEE Transactions on AES*, vol. 24, no. 4, July 1988.

[8] Trunk, G.V., "Range Resolution of Targets Using Automatic Detectors," *IEEE Transactions on Aerospace and Electronic Systems*, vol. AES-14, no. 5, September 1978.

[9] Rickard, J.T., and Dillard, G.M., "Adaptive Detection Algorithms for Multiple-Target Situations," *IEEE Transactions on Aerospace and Electronic Systems*, vol. AES-13, no. 4, July 1977.

[10] Ritcey, J.A., "Performance Analysis of the Censored Mean-Level Detector," *IEEE Transactions on Aerospace and Electronic Systems*, vol. AES-22, no. 4, pp. 443–454, July 1986.

[11] Rohling, H., "Radar CFAR Thresholding in Clutter and Multiple Target Situations," *IEEE Transactions on Aerospace and Electronic Systems*, vol. AES-19, no. 4, pp. 608–621, July 1983.

[12] Rohling, H., "New CFAR-Processor Based on an Ordered Statistic," pp. 271–275 in *Proceedings of the IEEE International Radar Conference,* Arlington, VA, 1985.

[13] Richards, M.A., *Fundamentals of Radar Signal Processing*, McGraw-Hill, New York, 2005.

[14] Kay, S.M., *Fundamentals for Statistical Signal Processing, vol. 1: Estimation Theory*, Prentice Hall, Englewood Cliffs, NJ, 1993.

[15] DiFranco, J.V., and Rubin, W.L., *Radar Detection*, Prentice-Hall, Englewood Cliffs, NJ, 1968.

[16] Beyer, W.H., *CRC Standard Mathematical Tables,* 26th ed., CRC Press, Boca Raton, FL, 1981.

[17] Elias-Fuste, A.R., "Analysis of Some Modified Ordered Statistic CFAR: OSGO and OSSO CFAR," *IEEE Transactions on Aerospace and Electronic Systems*, vol. 26, no. 1, pp. 197–201, January 1990.

[18] Ritcey, J.A., and Hines, J.L., "Performance of Max-Mean Level Detector with and without Censoring," *IEEE Transactions on Aerospace and Electronic Systems*, vol. AES-25, no. 2, pp. 213–222, March 1989.

[19] Wilson, S.L., "Two CFAR Algorithms for Interfering Targets and Nonhomogeneous Clutter," *IEEE Transactions on Aerospace and Electronic Systems,* vol. 29, no. 1, pp. 57–72, January 1993.

[20] Ritcey, J.A., and Hines, J.L., "Performance of MAX Family of Order-Statistic CFAR Detectors," *IEEE Transactions on Aerospace and Electronic Systems*, vol. 27, no. 1, pp. 48–57, January 1991.

[21] Finn, H.M., "A CFAR Design for a Window Spanning Two Clutter Fields," *IEEE Transactions on Aerospace and Electronic Systems*, vol. AES-22, no. 2, pp. 155–169, March 1986.

[22] Himonas, S.D., and Barkat, M., "A Robust Radar CFAR Detector for Multiple Target Situations," *Proceedings of the IEEE National Radar Conference,* pp. 85–90, 1989.

[23] Gandhi, P.P., and Kassam, S.A., "An Adaptive Order Statistic Constant False Alarm Rate Detector," pp. 85–88 in *Proceedings of the IEEE National Radar Conference,* 1989.

[24] Himonas, S.D., "Adaptive Censored Greatest-of CFAR Detection," *IEE Proceedings-F*, vol. 139, no. 3, pp. 247–255, June 1992.

[25] Himonas, S.D., and Barkat, M., "Automatic Censored CFAR Detection for Nonhomogeneous Environments," *IEEE Transactions on Aerospace and Electronic Systems*, vol. 28, no. 1, January 1992.

[26] Guida, M., Longo, M., and Lops, M., "Biparametric CFAR Procedures for Lognormal Clutter," *IEEE Transactions on Aerospace and Electronic Systems,* vol. 29, no. 3, pp. 798–809, July 1993.

[27] Schleher, D.C., "Harbor Surveillance Radar Detection Performance," *IEEE Journal of Oceanic Engineering,* vol. 2, no. 4, pp. 318–325, October 1997.

[28] Gandhi, P.P., Cardona, E., and Baker, L., "CFAR Signal Detection in Nonhomogeneous Weibull Clutter and Interference," pp. 583–588 in *IEEE International Radar Conference*, 1995.

[29] Ravid, R., and Levanon, N., "Maximum-Likelihood CFAR for Weibull Background," *IEE Proceedings–F,* vol. 139, no. 3, pp. 256–264, June 1992.

[30] Levanon, N., and Shor, M., "Order Statistics CFAR for Weibull Background," *IEE Proceedings–F,* vol. 137, no. 3, pp. 157–162, June 1990.

[31] Rifkin, R., "Analysis of CFAR Performance in Weibull Clutter," *IEEE Transactions on Aerospace and Electronic Systems*, vol. 30, no. 2, pp. 315–329, April 1994.

[32] Nitzberg, R., "Clutter Map CFAR Analysis," *IEEE Transactions on Aerospace and Electronic Systems,* vol. 22, no. 4, pp. 419–421, July 1986.

[33] Levanon, N., "Numerically Efficient Calculations of Clutter Map CFAR Performance," *IEEE Transactions on Aerospace and Electronic Systems,* vol. 23, no. 6, pp. 813–814, November 1987.

[34] Nathanson, F.E., *Radar Design Principles*, 2d ed., McGraw-Hill, Inc., New York, pp. 129–142, 1991.

16.12 PROBLEMS

1. A CFAR is designed to maintain a probability of false alarm equal to 10^{-6}. Detections are performed on a per pulse basis. The pulse repetition frequency is 1 kHz. During a pulse repetition interval, 2000 samples are collected in range. What is the false alarm rate?

2. For Rayleigh distributed interference with an average interference power of 2 mwatts per receiver channel (assume both I and Q channels are present), what is the threshold required to achieve a $P_{FA} = 10^{-4}$? Assume a Neyman-Pearson detector.

3. The Neyman-Pearson threshold is set to achieve a $P_{FA} = 10^{-6}$. The interference power level changes by 6 dB. What is the new P_{FA} if the threshold remains unchanged?

4. Calculate the average P_D for a CA-CFAR with $N = 20$ and $P_{FA} = 10^{-4}$ in a homogenous environment. Assume the target in the CUT has $SINR = 22$ dB.

5. Calculate the CFAR loss associated with a CA-CFAR. Assume $P_D = 0.85$, $P_{FA} = 10^{-6}$, and $N = 20$.

6. For a CA-CFAR, calculate the SINR required to achieve a $P_D = 0.95$, with $N = 16$ and $P_{FA} = 10^{-4}$ in a homogeneous environment.

7. For a CA-CFAR, calculate P_D with one interfering target in the reference window. Assume $N = 20$, $SINR_{CUT} = SINR_{IT} = 20$ dB, and $P_{FA} = 10^{-4}$.

8. Given a clutter boundary and the potential for clutter edge masking, what is the P_D associated with a target in the lower reflectivity region with $SINR = 20$ and $\Delta C = 15$ dB. Assume $P_{FA} = 10^{-5}$, $N = 20$, and five samples of the leading window appear in the higher reflectivity region.

9. Given a clutter boundary and the potential for a clutter edge false alarm, what is the P_{FA} when the CUT of a CA-CFAR lies in the higher reflectivity region with $\Delta C = 20$ dB? Assume $N = 14$, $P_{FA} = 10^{-4}$, and five samples of the lagging window appear in the lower reflectivity region.

10. For a GO-CA CFAR, which statement is true:

a. Reduces mutual target masking. Increases clutter edge false alarms.

b. Reduces both mutual target masking and clutter edge false alarms.

c. Reduces clutter edge false alarms. Increases mutual target masking.

11. A censored CFAR has a reference window containing the following samples at the output of a square law detector. Compute the CFAR statistic with $N_C = 3$. How many interferers is the CFAR capable of rejecting? Leading $= \{1.1, 0.5, 2.8, 0.8, 0.99, 0.3\}$, Lagging $= \{0.65, 0.29, 0.87, 1.6, 0.3, 1.6\}$

12. Using the reference window data in problem 11, compute the CFAR statistic for an order statistic CFAR with $k = 0.75N$. How many interferers is the CFAR capable of rejecting?

13. Using the reference window data in problem 11, compute the CFAR statistic for a CA, GOCA, and SOCA-CFAR. Use the sample mean to compute the statistic in each case. For the CA-CFAR, compute the threshold given a $P_{FA} = 10^{-6}$.

14. Using the reference window data in problem 11, compute the CFAR statistic for a GO-OS CFAR with $k = 4$.

15. Given a scenario where at most three targets may appear in the reference window, which algorithm provides the most robustness to target masking? Assume $N = 16$.

a. Censored CFAR, $N_C = 2$.

b. Order Statistic CFAR, $k = 14$.

c. Greater-of CA-CFAR.

d. Smaller-of CA-CFAR.

e. Order Statistic CFAR, $k = 12$.